Aida Andreia Pereira Pires Lima

Licenciada em Biologia

Identifying new regulators of the actin cytoskeleton in endothelial tip cells

Dissertação para obtenção do Grau de Mestre em
Genética Molecular e Biomedicina

Orientador: Cláudio Areias Franco, PhD, iMM Lisboa

Júri:

Presidente: Prof. Doutora Paula Maria Theriaga Mendes Bernardo Gonçalves

Arguente: Doutora Maria Leonor Tavares Saúde

Vogal: Doutor Cláudio Areias Franco

FACULDADE DE CIÊNCIAS E TECNOLOGIA
UNIVERSIDADE NOVA DE LISBOA

Setembro 2015

Aida Andreia Pereira Pires Lima

Licenciada em Biologia

Identifying new regulators of the actin cytoskeleton in endothelial tip cells

Dissertação para obtenção do Grau de Mestre em
Genética Molecular e Biomedicina

Orientador: Cláudio Areias Franco, PhD, iMM Lisboa

Júri:

Presidente: Prof. Doutora Paula Maria Theriaga Mendes Bernardo Gonçalves

Arguente: Doutora Maria Leonor Tavares Saúde

Vogal: Doutor Cláudio Areias Franco

FACULDADE DE CIÊNCIAS E TECNOLOGIA
UNIVERSIDADE NOVA DE LISBOA

Setembro 2015

Identifying new regulators of the actin cytoskeleton in endothelial tip cells

Para o meu pai,

Quando te sentires perdida, confusa, pensa nas árvores, lembra-te da forma como crescem. Lembra-te de que uma árvore com muita ramagem e poucas raízes é derrubada à primeira rajada de vento, e de que a linfa custa a correr numa árvore com muitas raízes e pouca ramagem. As raízes e os ramos devem crescer de igual modo, deves estar nas coisas e estar sobre as coisas, só assim poderás dar sombra e abrigo, só assim, na estação apropriada, poderás cobrir-te de flores e de frutos.

(Susanna Tamaro)

ACKNOWLEDGMENTS

Quero começar por agradecer ao meu orientador, Cláudio Areias Franco, por me ter aceite a responsabilidade científica deste trabalho e pela dedicação e exigência com que sempre seguiu este projecto. Obrigada por todos os desafios que me foi colocando ao longo do tempo, que possibilitaram não só uma grande aprendizagem e espírito crítico ao longo do trabalho, mas também me ajudaram a ser mais segura e persistente comigo própria, principalmente na questão do inglês ☺ . Por tudo isto, espero ter estado à altura das oportunidades que me ofereceu. E claro, a esta grande instituição que é o Instituto de Medicina Molecular, onde sem ela nada disto seria possível.

Aos meus colegas de trabalho, Joana Carvalho e Pedro Barbacena por todo o apoio e auxílio prestado na revisão desta dissertação e principalmente amizade e companhia sempre concedidos. Sim e não me esqueci, um agradecimento especial à minha colega Catarina que não só foi uma óptima colega de trabalho, em todos os sentidos, mas também se tornou uma grande amiga que espero manter para toda a vida ☺

Um agradecimento especial a duas grandes amigas Ana Alves e Lucília Pereira. À Ana não só por ter dado início a este projecto, mas também porque é uma amiga que muito antes já estava no meu coração e que sempre me deu todo o apoio e carinho. À Lucília, que nem tenho palavras para descrever todo o apoio e profunda amizade que me deu ao longo deste período tão importante, e principalmente, por sempre acreditar em mim.

Às minhas amigas Raquel Nisa, Márcia Silva e Daniela Moreira pelo carinho e amizade dados ao longo destes anos, não esquecendo deste tão importante na minha carreira de investigação.

À Sara Moreira que não só foi uma grande colega neste mestrado, como também se tornou uma amiga que sempre me deu apoio, bastando apenas um SMS ☺

Ao meu irmão pela confiança depositada em mim e por todo o amor concedido que me ajudou a enfrentar esta etapa importante da minha vida.

Por último, mas na verdade o primeiro, AO MEU PAI a quem não só dedico esta tese, mas também a quem agradeço do fundo do meu coração que mesmo não estando “presente” sempre me deu apoio durante todos os momentos mais difíceis neste projecto e que muitas vezes me puseram a pensar em desistir. OBRIGADA PAI <3

Em geral, a todas as outras pessoas que acompanharam o meu trajecto académico e/ou pessoal e que de alguma forma estiveram envolvidos neste projecto, permitindo que este fosse possível.

ABSTRACT

Blood vessels form extensive vascular networks allowing an efficient transport of gases, fluids and nutrients for all tissues. Sprouting angiogenesis generates new blood vessels during embryonic development and adult. Dysfunctional, either excessive or insufficient, angiogenesis is a cause of several vascular diseases, such as ischemia, arteriovenous malformations, tumor angiogenesis, and diabetic retinopathy.

During sprouting angiogenesis, endothelial tip cells are highly migratory and guide the trailing endothelial stalk cells in the nascent sprout towards the source of pro-angiogenic factors. However, the mechanisms regulating the actin cytoskeleton contributing to the motility and invasive proprieties of endothelial tip cells are poorly understood. Serum response factor (SRF) is a transcription factor that regulates expression of genes encoding cytoskeletal proteins. SRF, together with its cofactors [myocardin related transcription factors (MRTFs)], is essential for tip cell migration and invasion during sprouting angiogenesis. But which genes downstream of SRF/MRTF signaling are central in this process are completely not characterized.

Based on a microarray approach, we defined the MRTF/SRF-dependent transcriptome of endothelial cells. Using a combination of multiple *in silico* and *in vitro* approaches, we identified the relevant genes downstream of SRF signaling, and we characterize their function in cell migration and cytoarchitecture of endothelial cells.

From our analysis, inhibition of MYH9, the gene coding for myosin IIA heavy chain (NMII-A), reproduced alone the full spectrum of phenotypes presented in MRTF/SRF-deficient endothelium, and regulates tip cell motility and invasion. Interestingly, we found a specialized localization of MYH9 in endothelial tip cells, pointing towards an important and novel role in filopodia formation and/or stability.

Our research provides new insights on the biology of endothelial tip cells, which can be a first step towards new therapeutic approaches targeting pathological vascularization.

Keywords: Angiogenesis; SRF signaling; MYH9; invasion; filopodia; tip cell

RESUMO

Os vasos sanguíneos formam uma extensa rede vascular que permite o eficiente transporte de gases, fluidos e nutrientes para todos os tecidos. A formação de novos vasos sanguíneos durante o desenvolvimento embrionário e no adulto ocorre pelo processo de angiogénese por brotação. Uma angiogénese disfuncional, excessiva ou insuficiente, é a causa de várias doenças, como isquemia, malformações arteriovenosas, angiogénese tumoral ou retinopatia diabética.

Na angiogénese por brotação, as células de ponta são altamente migratórias, e orientam a invasão do broto vascular. No entanto, os mecanismos de regulação do citoesqueleto de actina envolvidos na motilidade e invasão das células de ponta são pouco compreendidos. O fator de resposta ao soro (SRF) regula a expressão de proteínas do citoesqueleto. SRF, em conjunto com os seus co-fatores [fatores de transcrição relacionados com miocardina (MRTFs)], é essencial para a migração e invasão das células de ponta durante a angiogénese. Porém os genes regulados pela sinalização SRF/MRTF que promovem estes efeitos ainda não foram caracterizados.

Usando *microarray,* definimos o transcriptoma das células endoteliais dependente da sinalização MRTF/SRF. Através de abordagens *in silico* e *in vivo,* identificámos os genes mais relevantes na via sinalização do SRF, e caracterizámos os seus efeitos no processo de migração e na citoarquitetura das células endoteliais.

O nosso estudo identificou que a inibição do gene MYH9, que codifica para a cadeia pesada da miosina IIA (NMII-A), leva a fenótipos similares à inibição da via MRTF/SRF, regulando a motilidade e invasão das células de ponta. Curiosamente, observámos uma localização particular da MYH9 nas células de ponta, apontando para um papel importante e novo da MYH9 na formação e/ou estabilidade dos filopódes.

Os nossos resultados fornecem novas pistas sobre a biologia das células endoteliais de ponta, constituindo um primeiro passo no sentido de desenvolver novas abordagens terapêuticas contra a vascularização patológica.

Termos-chave: angiogénese; sinalização SRF/MRTF; MYH9; invasão; filopódes; célula de ponta

TABLE OF CONTENTS

ACKNOWLEDGMENTS ..... **IV**
ABSTRACT ..... **VII**
RESUMO ..... **IX**
I. INTRODUCTION **1**
1. Blood Vessels 1
1.1. Vascular Networks 1
1.2. Vascular Diseases 2
2. Sprouting angiogenesis 2
2.1.General concepts on angiogenesis 2
2.2. Hypoxia and VEGF signaling 3
2.3. VEGF and Notch signaling 4
2.4. Tip and Stalk cell specification 4
2.5. Basement membrane degradation and mural cells detachment 6
2.6. Lumen formation 7
2.7. Sprout anastomosis 8
2.8. Vessel Maturation 9
2.9. Endothelial cell motility 10
3. Actin cytoskeleton in motile cells 10
3.1. Cytoskeleton dynamics 10
3.2. Filopodia and lamellipodia protrusions 11
3.3. Actin/Myosin interactions 13
4. Serum Response Factor (SRF) 15
4.1. Molecular and biological functions of SRF 15
4.2. Actin-MRTF-SRF signaling 16
4.3. SRF function in sprouting angiogenesis 17
5. Working Models for studying vascular development 18
5.1. Mouse retinal model 18
5.2. Spheroid sprouting assay 19
6. Aims 19

II. MATERIALS AND METHODS **21**
1. Mice breeding and genotyping 21
2. Culture of Human Umbilical Vein Endothelial Cells (HUVECs) 22
3. VEGF induction in HUVECs 22
4. siRNA experiments 23
5. Overexpression of MIIA-GFP in SRF depleted HUVECs 24
6. Gene expression assays 24

7. Protein extraction and Western Blotting 25
7.1. Protein lysis and sample processing 25
7.2. Protein electrophoresis and membrane transference 26
8. Scratch-wound assay 26
9. Immunofluorescence staining of cultured HUVECs in coverslips 26
10. Eyes extraction and retina isolation for immunoflorescence 27
10.1. Immunofluorescence staining in whole-mount retinas 28
11. Antibodies and other molecular probes 29
12. Spheroids sprouting assay 30
12.1. Methyl cellulose stock solution 30
12.2. Sprouting angiogenesis *in vitro* 30
12.3. Immunofluorescence staining of Spheroids 32
13. Statistical analysis 32

III. RESULTS 33
1. Selection of candidate genes downstream of the MRTF/SRF pathway 33
1.1. Transcriptomic analysis of endothelial-specific MRTF/SRF-dependent genes 33
1.2. Validation of MRTF/SRF-dependent candidate genes 35
2. Functional validation of positive candidate genes 36
2.1. Setting-up a siRNA-based functional screen 36
2.2. Scratch-wound cell migration assay 38
2.3.Cell Cytoskeleton architecture 40
3. MYH9 is a major actin regulator downstream of the MRTF/SRF pathway 42
3.1. MYH9 function is essential for efficient endothelial sprouting 42
3.2. Re-expression of MYH9 rescues SRF-deficient phenotype 45
3.3. MYH9 is enriched in endothelial tip cells *in vivo*. 46

IV. DISCUSSION 47

V. REFERENCES 51

INDEX OF FIGURES

I. INTRODUCTION……....1
Figure I.1 - Schematic representation of vascular network formation.. 1
Figure I.2 - Mechanisms of sprouting and non-sprouting angiogenesis. 3
Figure I.3 - Molecular mechanism regulating ECs selection into a tip and stalk cells during sprouting angiogenesis.. 6
Figure I.4. - Schematic representation of sprouting angiogenesis initiation, vessel branching, and maturation.. 7
Figure I.5 - Lumen formation during sprout outgrowth. 8
Figure I.6 - Schematic illustration of anastomosis process, during tip cell fusion. 9
Figure I.7 - Schematic representation of the cell with the different architectures in the motile cell. 11
Figure I.8 - Structural elements of a migrating cell.. 12
Figure I.9 - Working model for filopodia formation. 13
Figure I.10 - Structure of non-muscle myosin II (NM II) and dynamics. 14
Figure I.11 - Model illustrating the two main pathways regulating SRF activity. 16
Figure I.12 - Schematic illustration of a growing sprout in mouse retina. 19

II. MATERIALS AND METHODS……....21
Figure II.1 - Tamoxifen injection, eye and retina dissection.. 28
Figure II.2 - Scheme of generation of spheroids.. 31

III. RESULTS……33
Figure III.1 - Venn Diagram for downstream of the MRTF/SRF signaling.. 33
Figure III.2 - Gene Ontology analysis for the 113 selected genes. 33
Figure III.3 - qPCR analysis of selected candidate genes. 35
Figure III.4 - Western Blot analysis of some the selected candidate genes.. 36
Figure III.5 - Analyze of the efficiency of each siRNA by qPCR. 37
Figure III.6 - Analysis of cell migration in the scratch-wound assay.. 38
Figure III.7 - Analysis of cell migration in the scratch wound assay.. 39
Figure III.8 - Analysis of cell migration in the scratch wound assay.. 41
Figure III.9 - Quantification of the fluorescence intensity of the different markers in HUVECs transfected with selected siRNAs.. 42
Figure III.10 - MYH9 staining in HUVECs transfected with selected siRNAs.. 43
Figure III.11 - Relative protein levels in HUVECs transfected with different siRNAs.. 43
Figure III.12 - HUVEC spheroid sprouting analysis. 44
Figure III.13 - Overexpression of MYH9-GFP compensates SRF-deficiency.. 45
Figure III.14 - Retinal endothelial cells analysis.. 46

IV. DISCUSSION……....47
Figure IV.1 - Schematic representation of SRF signaling inducing NMII-A activity. 49

INDEX OF TABLES

II. MATERIALS AND METHODS……21
Table II.1 - Primers used for genotyping PCR.....21
Table II.2 - Genotyping PCR program.....22
Table II.3 - siRNA sequences used in siRNA experiments. 23
Table II.4 - Lipofectamine® LTX DNA Transfection Protocol. 24
Table II.5 - Primers used in qPCR.....25
Table II.6 - Primary antibodies used and respective information 29
Table II.7 - Secondary antibodies and Phalloidin used and respective information.....30
Table II.8 - Collagen I solution for sprouting angiogenesis assay.....31

III. RESULTS……33
Table III.1 - Selected candidate genes.....34
Table III.2 - Viability tests in cultured HUVECs.. 37

I. INTRODUCTION

1. Blood Vessels

1.1. Vascular Networks

Blood vessels form extensive vascular networks, allowing an efficient and simultaneous transport of gases, fluids, nutrients, signaling molecules and circulating cells between all the organs of the vertebrate body (Herbert and Stainier, 2011; Adams and Alitalo, 2007). The vertebrate circulatory system includes two highly branched, tree-like tubular networks: the blood vessels and the lymphatic vessels. These two endothelial networks are interconnected, which allows the drainage of lymph into the blood circulation (Adams and Alitalo, 2007; Carmeliet, 2005) (Figure I.1).

Early embryonic blood vessels form *de novo* via the assembly of mesoderm-derived endothelial cell precursors, referred by angioblasts, which form from hemangioblasts (differentiated from mesodermal cells). The hemangioblasts form aggregates in the yolk sac. The inner cells differentiate into hematopoietic precursors, whereas the outer population into endothelial cells (angioblasts) that migrate and form a primitive vascular network. This step of vascular development is named by vasculogenesis (Potente *et al.*, 2011; Carmeliet, 2005) (Figure I.1). Subsequently, the primitive vascular plexus progressively expands and remodels, leading to the formation of a mature and functional hierarchical vascular network, composed by arteries, veins and capillaries, a process defined as angiogenesis (Herbert and Stainier, 2011; Carmeliet, 2005) (Figure I.1).

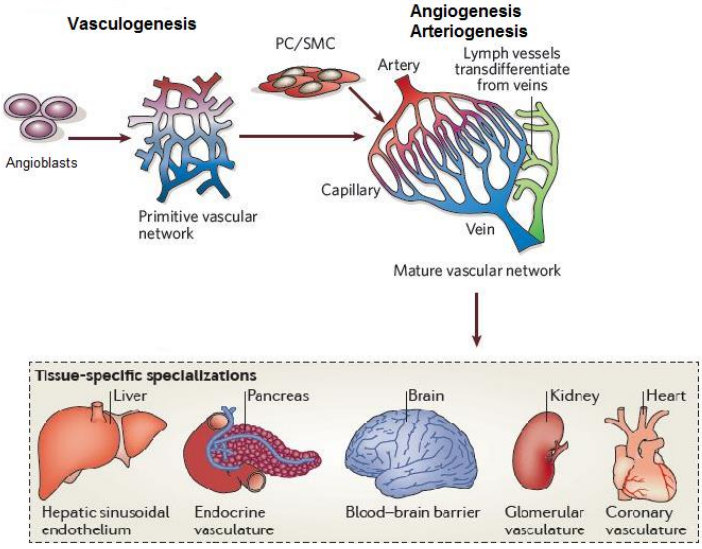

Figure I.1 - Schematic representation of vascular network formation. Once formed, in vasculogenesis, hemangioblasts differentiate in endothelial cells (ECs) in order to form an immature and primitive vascular network. Following their vasculogenic assembly this primary plexus expands, remodels and matures into a mature and hierarchical vascular network consisting of arteries, veins and capillaries (angiogenesis and arteriogenesis). Recruitment of mural cells [pericytes (PCs) and vascular smooth-muscle cells (vSMCs)] stabilizes nascent vessels and promotes vessel maturation. In addition, the sprouting of lymphatic endothelial cells from venous vessels (lymphangiogenesis) seeds the lymphatic system that interconnects with blood vessels. This vascular network diversity is further augmented by tissue-specific specializations that alter key properties to generate vascular networks with new molecular signatures. Figure adapted from Herbert and Stainier (2011), and Carmeliet (2005).

1.2. Vascular Diseases

Blood vessels supply oxygen, nutrients and are also involved in immune surveillance. Thus, it is not surprising that defective blood vessel formation, maintenance or growth contribute to the onset of many diseases such as ischemia, myocardial infarction, stroke, ulcerative diseases, neurodegenerative or obesity-associated disorders (Potente *et al.*, 2011; Carmeliet and Jain, 2011; Carmeliet, 2003). In contrast, when excessive vascular growth or abnormal remodeling is linked to other diseases such as tumor growth and metastasis, inflammatory disorders, pulmonary hypertension, and retinopathies (Potente *et al.*, 2011; Carmeliet and Jain, 2011; Carmeliet, 2003).

Ischemia-related damages depend on several factors, such as the extent of the ischemic injury, the duration of ischemia and the efficiency of reperfusion. Therefore, *de novo* formation of microvessels by angiogenesis limits the consequences of ischemic myocardium, by reperfusing the hypoxic tissue (Cochain *et al.*, 2013). In ischemic retinopathies, including proliferative diabetic retinopathy (PDR) and retinopathy of prematurity (ROP), an initial phase of retinal capillary obliteration is followed by hypoxia that drives deregulated, excessive and pathological growth of new blood vessels, but without ameliorating retinal ischemia. Sustained hypoxia further exacerbates pathological angiogenesis, causing severe hemorrhages, retinal detachment and blindness. These eye-related vascular diseases are managed using anti-angiogenic therapies, with great clinical outcomes (Fukushima *et al.*, 2011).

Tumor growth and spread of tumor cells (metastasis) requires angiogenesis. Growth of tumors depends on induction of formation of new blood vessels for adequate oxygen and nutrient supply. The medical community has been using anti-angiogenic therapy to starve tumor cells, by cutting access to supply of oxygen and nutriments. However, tumors rapidly become resistant to single-target anti-angiogenic therapies, evolving new mechanisms promoting vessel growth. Thus, the scientific community needs to discover new methods to improve the overall efficiency of anti-vascular strategies to combat cancer (Potente *et al.*, 2011).

2. Sprouting angiogenesis

2.1. General concepts on angiogenesis

The term “angiogenesis” was first used to describe the formation of new blood vessels from pre-existing ones but, recently, this term is used to generally denote the growth and remodeling process of the primitive vascular network into a hierarchical and functional one (Potente *et al.*, 2011; Carmeliet, 2000). There are two different mechanisms of angiogenesis: sprouting and intussusceptive angiogenesis (non-sprouting). Intussusceptive angiogenesis defines the process of splitting pre-existing vessels in two separate ones. This process involves the formation of transluminal tissue pillars within capillaries, small arteries, and veins, which subsequently fuse. This invagination creates contact of opposing endothelium walls and results in the formation of transluminal pillar accompanied by vessel growth. Thus, new vascular entities or vessel remodeling can occur in non-sprouting angiogenesis (Heinke *et al.*, 2012; Potente *et al.*, 2011; Makanya *et al.*, 2009) (Figure I.2).

Sprouting angiogenesis refers to the formation of new vessels from pre-existing ones, in which endothelial cells are activated and selected to sprout. The major difference between both mechanisms

is that sprouting angiogenesis is invasive to non-vascularized tissues, relatively slow and is highly dependent on cell proliferation. In contrast, the process of intussusception allows the formation of new blood vessels rapidly, and does not rely on cell proliferation to expand the existing capillary networks. Nevertheless, sprouting angiogenesis is the process that accounts for the vast majority of vascular growth and it will be explained in greater detail in the next section (Graupera and Potente, 2013; Heinke et al., 2012).

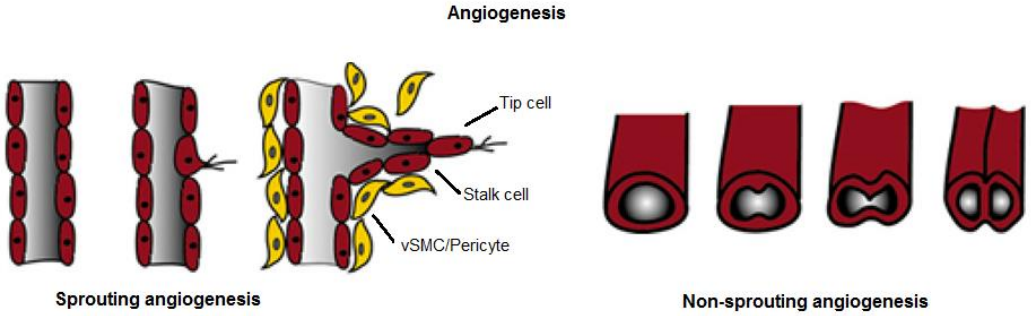

Figure I.2 - Mechanisms of sprouting and non-sprouting angiogenesis. During angiogenesis, the primary vascular plexus expands by two mechanisms of sprouting (left) and non-sprouting angiogenesis (right). Sprouting of vessels from pre-existing ones in which endothelial cells proliferate behind the tip cell of growing branch, and non-sprouting involved in transluminal pillar formation and growing of vessels. Figure adapted from Heinke *et al.* (2012).

2.2. Hypoxia and VEGF signaling

Sprouting angiogenesis occur during embryonic development and in the adult and comprises several steps. Biological signals such as hypoxia, ischemia, and/or blood vessel damage promote the upregulation of pro-angiogenic growth factors that activate their corresponding receptors (Zimna and Kurpisz, 2015). Thus, regulation of angiogenesis by hypoxia is an important component of homeostatic mechanisms that link vascular oxygen supply to metabolic demand (Pugh and Ratcliffe, 2003). Hypoxia-inducible factor-1 (HIF-1) is a primary transcriptional mediator of the hypoxic response and is the master regulator of oxygen homeostasis (Semenza, 2003). This is a heterodimer consisting of HIF-1α and HIF-1β subunits. The HIF-1α subunit is stabilized by hypoxia, whereas the HIF-1β subunit is a constitutive nuclear protein (Pugh and Ratcliffe, 2003).

Current studies have indicated that hypoxia and HIF-1 expression plays a critical role in stimulating ECs and promoting angiogenesis by:

(1) Activating transcription of genes encoding angiogenic growth factors, including vascular endothelial growth factor A (VEGF-A), angiopoietin 2 (ANGPT2), placental growth factor (PLGF), and platelet-derived growth factor B (PDGFB);

(2) Regulating pro-angiogenic cytokines and receptors;

(3) Controlling the transcription of genes involved in endothelial cell proliferation and division (Zimna and Kurpisz, 2015; Manalo *et al.*, 2005).

Therefore, in hypoxic conditions, the vessel formation cascade is supported by HIF-1 that participates directly on all the fundamental steps of angiogenesis. Direct binding of HIFs to specific hypoxia-inducible elements (HRE), present in the promoter region of VEGF-A leads to a dramatic upregulation of VEGF-A production. Thus, HIF-1 is a master regulator of VEGF levels, linking directly hypoxia to angiogenesis, in a system regulated by the simple rule of demand and supply (Zimna and Kurpisz, 2015; Olsson *et al.*, 2006; Pugh and Ratcliffe, 2003).

2.3. VEGF and Notch signaling

The VEGF family of growth factors includes six secreted dimeric glycoproteins (VEGF-A, -B, -C, -D, -E, and placental growth factor [PLGF]), which interact with distinct affinities with three different tyrosine kinase receptors, VEGF receptor 1 (VEGFR1 or Flt1), receptor 2 (VEGFR2, KDR or Flk1), and receptor 3 (VEGFR3 or Flt4). VEGFR1 and VEGFR2 are involved in the regulation of vasculogenesis and angiogenesis, whereas VEGFR3 is involved in embryonic angiogenesis but later becomes confined to lymphangiogenesis (Blanco and Gerhardt, 2013; Potente *et al.*, 2011).

A key molecule for the initiation and direction of sprouting is VEGF-A (Eilken and Adams, 2010). VEGF-A expression is induced by hypoxic conditions, cytokines, growth factors, hormones, oncogenes, and tumor-suppressor genes (Blanco and Gerhardt, 2013). The tyrosine kinase activity of VEGFR2 is the main mediator of VEGF-A signaling during angiogenesis. Contrary to VEGFR2, VEGFR1 has a rather feeble kinase activity and acts as a decoy receptor, competitively reducing VEGF-A binding to VEGFR2, and therefore limiting its activity of VEGF-A pathway in endothelial cells (Blanco and Gerhardt, 2013). Extracellular gradients of VEGF-A activate quiescent endothelial cells from blood vessels and induce their subsequent specialization into tip and stalk cells.

2.4. Tip and Stalk cell specification

As previously explained, hypoxic tissues secrete growth factors and chemokines that stimulate endothelial cells to abandon their stable position in the vessel wall. Jointly, endothelial cells undergo coordinate sprouting and branching. The sequence of the morphogenic events occurring during sprouting angiogenesis requires the tight control and coordination of endothelial cell behavior that will ensure not only the formation of new sprouts, but also the maintenance of a functional vascular network. During the process of sprouting angiogenesis, there are two different endothelial cell populations of upmost importance (Siekmann *et al.*, 2013; Potente *et al.*, 2011; Adams and Alitalo, 2007):

(1) **The leading tip cells:** specialized cells selected for sprouting that are highly motile and invasive. Tip cells are able to sense both attractive and repulsive cues from the environment and have characteristic dynamic long filopodia protrusions, which control the guidance of newly formed vascular sprouts;

(2) **The following stalk cells:** these cells are in close contact to tip cells and constitute the base of the sprout. Stalk cells proliferate while establishing firm adherent and tight junctions in order to maintain the connection to the parental vessel.

Tip and stalk cells not only differ in their behavior and morphology, but also display remarkable differences in their gene expression signature. Whereas tip cells highly express *VEGFR2*, *VEGFR3*, *PDGFB*, *ANG2*, *UNC5B*, *ESM1*; *CXCR4*, and Nidogen-2, stalk cells express higher levels of *Robo4*, *Jagged1*, and *VEGFR1*. These gene expression differences determine their specialized functions during sprouting angiogenesis *(*Potente *et al.*, 2011; Phng and Gerhardt, 2009).

The selection of endothelial cells into tip and stalk cells is controlled by delta-like 4 (Dll4)–Notch signaling through a phenomenon known as lateral inhibition. Tip cells have higher levels of Dll4, compared with stalk cells, which are subjected to higher levels of Notch signaling. Although endothelial cells express several Notch receptors, Notch1 is critical for suppressing the tip cell phenotype in stalk cells (Hellström *et al.*, 2007). VEGFR activity affects expression of the Notch ligand Dll4. It is also known that Notch signaling influences the level of VEGFRs, suggesting that relative differences in VEGFR levels between adjacent cells may explain how Notch signaling controls sprouting. Thus, these observations indicate that these two pathways interconnect in an intercellular VEGF–VEGFR–Dll4–Notch–VEGFR feedback loop, that is necessary and sufficient to stably pattern endothelial cells into tip and stalk cells under adequate VEGF-A stimulation. Dll4 ligand induces the activation of Notch in neighboring endothelial cells, leading to the inhibition of the tip cell phenotype in these cells by downregulating VEGFR2, VEGFR3, and NRP1, while upregulating VEGFR1. On the contrary, cells with lower VEGFR1 expression start to compete for the tip cell position (Blanco and Gerhardt, 2013; Potente *et al.*, 2011; Jakobsson *et al.*, 2010; Phng and Gerhardt, 2009) (Figure I.3). Unlike Dll4 that is mainly expressed by tip cells the Notch ligand Jagged1 (JAG1) is expressed primarily by stalk cells. This ligand is a pro-angiogenic regulator that antagonizes Dll4–Notch signaling, and thereby positively controls the number of sprouts and tips. In addition, post-translational modifications of Notch receptors mediated by Fringe-family enzymes favors the Dll4-mediated Notch activation, but strongly decrease the signaling capability of Jagged1. Therefore, Fringe is critical for the opposing roles of Jagged1 and Dll4 during tip and stalk cell selection (Potente *et al.*, 2011; Eilken and Adams, 2010) (Figure I.3).

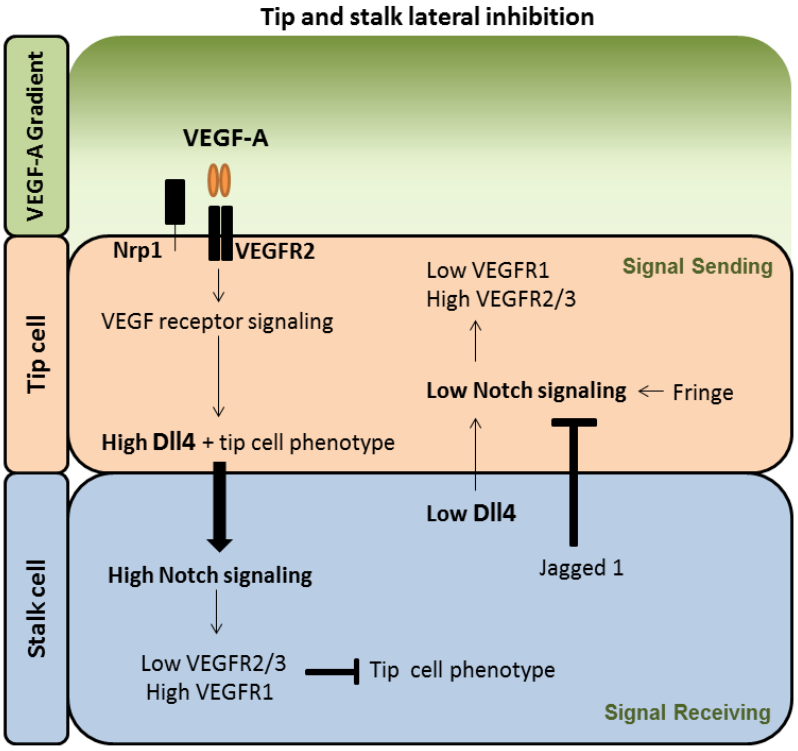

Figure I.3 - Molecular mechanism regulating ECs selection into a tip and stalk cells during sprouting angiogenesis. The specification of ECs into tip and stalk cells is controlled by VEGF and Notch signaling pathways. VEGF-A interacts with VEGFR2. Nrp1 modulates the VEGF-A signaling output, enhancing the binding activity and signaling of VEGF-A through VEGFR2. Under VEGF-A stimulation, Dll4 expression is up-regulated in the tip cells, and Dll4 ligand activates Notch that, consequently, suppressing the tip cell phenotype. Notch signaling activation reduces VEGFR2/3 expression and increases VEGFR1 levels. In contrast, the tip cell receives low Notch signaling, allowing high expression of VEGFR2/3 and Nrp1, but low VEGFR1. Contrary to Dll4, Jagged1 ligand is expressed by the stalk cells and antagonizes Dll4–Notch signaling in the sprouting front when the Notch receptor is modified by the glycosyltransferase Fringe, thereby enhancing differential Notch activity between tip and stalk cells. Figure created based in Blanco and Gerhardt (2010).

2.5. Basement membrane degradation and mural cells detachment

The first processes occurring during the generation of new sprouts in response to VEGF are the degradation of basement membrane and mural cells detachment that support cells in quiescent blood vessels. Endothelial and mural cells (vSMCs and pericytes) share a basement membrane composed of extracellular matrix (ECM) proteins that wrap around endothelial tubules. This ECM and mural cells are essential to prevent endothelial cells from leaving their positions (Potente *et al.*, 2011).

At the beginning of the sprouting process, the basement membrane components are degraded by proteolytic degradation. This controlled degradation is performed by matrix metalloproteases (MMPs), which are enriched in endothelial tip cells. In the other hand, the detachment of mural cells is stimulated by the release of ANGPT2 from endothelial cells, destabilizing the quiescent vasculature and therefore promoting sprouting angiogenesis (Potente *et al.*, 2011; Huang *et al.*, 2010) (Figure I.4).

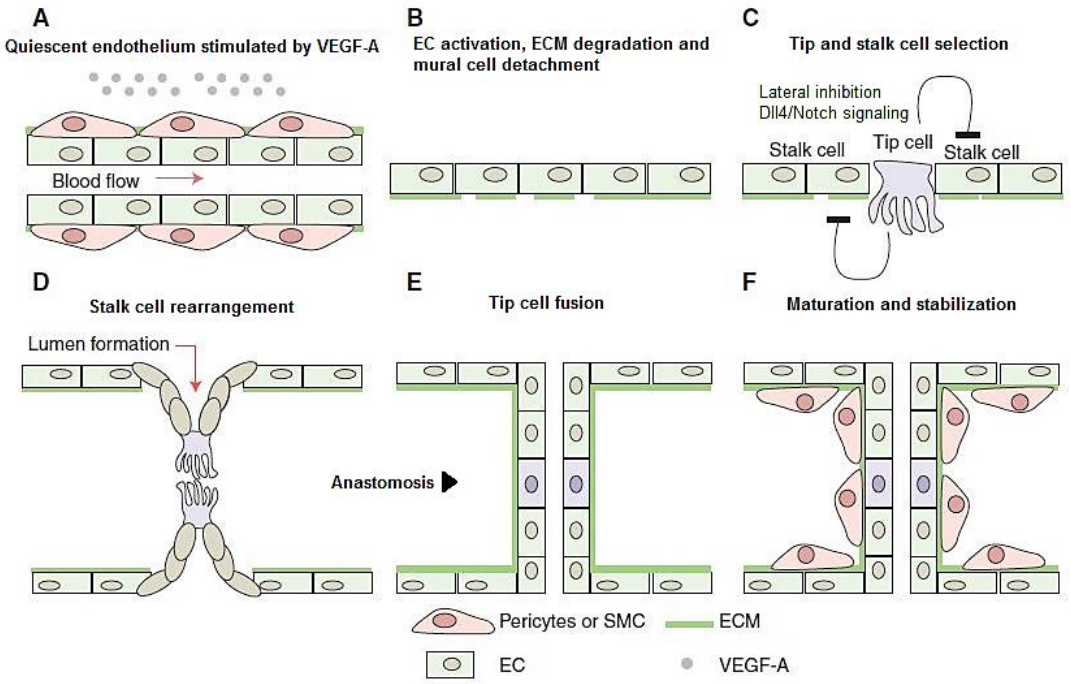

Figure I.4. - Schematic representation of sprouting angiogenesis initiation, vessel branching, and maturation. Angiogenesis is activated in response to hypoxic tissue that releases VEGF-A. **A**, VEGF-A stimulate the activation of quiescent ECs. **B**, At the cellular level, the angiogenic initiation requires the degradation of basement membrane and detachment of mural cells. **C**, also the specification of the activated ECs into tip and stalk cells is requires. **D**, ECs proliferate and collectively invade the hypoxic tissue while they remain connected to the original vascular network. In the nascent sprout characterized by their migratory behavior and dynamic filopodia, tip cells guide the sprout, followed by stalk cells, which proliferate and support the sprout elongation. **E**, tip cells forms the new connection into a functional vessel loop, between different sprouts through tip cell fusion (anastomosis). Formation of the vascular lumen allows the blood flow, increases tissue oxygenation, and reduces the release of endothelial growth factors, supporting the establishment of quiescence blood vessel. **F**, vessel maturation and stabilization proceed is initiated, with the recruitment of mural cells and the deposition of basement membrane. Figure adapted from Blanco and Gerhardt (2010).

2.6. Lumen formation

Other important role of the stalk cells during angiogenesis is the establishment of a vascular lumen in the newly formed blood vessel. This process can occur by different mechanisms depending on the vascular plexus or type of vessel that forms. Three mechanisms, including budding, cord hollowing, and cell hollowing can operate in vascular endothelial cells during development or post-natal angiogenic events (Potente *et al.*, 2011; Geudens and Gerhardt, 2011; Iruela-Arispe and Davis, 2009).

Studies in intersomitic vessels (ISVs) of zebrafish indicate that endothelial cells form a lumen by coalescence of intracellular (pinocytic) vacuoles, which interconnect with vacuoles from neighboring endothelial cells to form continuous multicellular lumenized tubule structures in a process known as cell hollowing (Potent *et al.* 2011). According to Iruela-Arispe and Davis, budding and cord hollowing may be essentially synonymous in angiogenic sprouting (Iruela-Arispe and Davis, 2009). In this case, and contrary to cell hollowing, endothelial cells can adjust their shape and rearrange their junctions to open up a lumen, with relocalization of junctional proteins and, consequently, cell shape modifications.

When undergoing cord hollowing, stalk cells, first, acquire an initial apical-basal polarity with VE-cadherin that also promotes the relocalization of CD34-sialomucins to the cell-cell contact sites. After this initial step, the negative charge of the sialomucins induces electrostatic repulsion signals in the apical (lumenal) membrane, promoting the initial separation of the apical membranes. During cell separation and extension of the lumen, endothelial cell adherents junctions are predominantly maintained by VE-cadherin, while adherent vascular endothelial molecules VE-cadherin-expressing junctions are relocalised to the lateral cell contact sites. Subsequent changes in endothelial cell shape and further separation of the adjacent endothelial cells and lumen expansion, are driven by VEGF that, in its turn, regulates the localization of non-muscle myosin II to the apically enriched F-actin cytoskeleton (Potente *et al.*, 2011; Geudens and Gerhardt, 2011; Iruela-Arispe and Davis, 2009) (Figure I.5). These changes are essential for establishment of vascular lumen formation allowing the initiation of new blood vessel formation.

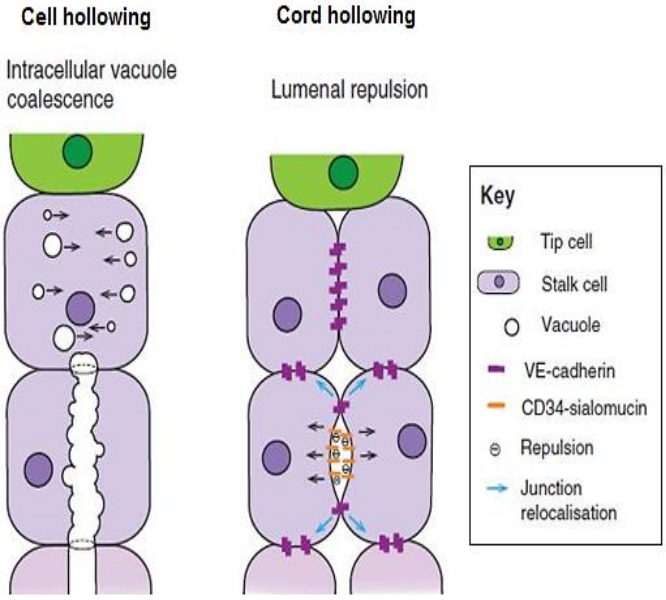

Figure I.5 - Lumen formation during sprout outgrowth. Left, cell hollowing, endothelial cells can form a lumen by forming intracellular vacuoles that coalesce and connect with each other and with vacuoles in neighboring cells. Right, cord hollowing, an intercellular lumen can be created by apical membrane repulsion. VE-cadherin establishes the initial apical-basal polarity and localizes CD34-sialomucins to the cell-cell contact sites. The negative charge of the sialomucins induces electrostatic repulsion and initial separation of the apical membranes, allowing the relocalization of junctional proteins to the lateral membranes (adapted from Geudens and Gerhardt (2011).

2.7. Sprout anastomosis

To generate new blood vessels, tip cells need to contact with other tip cells and assemble new lumen containing tubules in order to add new vessel circuits to the existing network through a process known as sprout anastomosis. The formation of new vascular connections by sprout anastomosis also requires that tip cells suppress their motile and explorative behavior, while maintaining strong adhesive interactions. Upon encountering their targets, the tip cells of other sprouts or existing capillaries, will establish new endothelial cell–endothelial cell junctional contacts, which are the first step of anastomosis (Adams and Alitalo, 2007). Later on, when the contact between tip cells is established, the adherent molecule VE-cadherin is recruited to the contact sites not only to consolidate the connection between the sprouts, but also to contribute for the downregulation of pro-angiogenic signaling and tip cell behavior at these sites (Potente *et al.*, 2011; Eilken and Adams, 2010; Vestweber, 2008) (Figure I.6). Besides VE-cadherin, macrophages are also known to support vessel anastomosis at sites of vessel fusion by accumulating and interacting with filopodia of neighboring tip

cells, and remaining in contact with vessel junctions after vessel sprouts fusion to form a vascular intersection (Potente *et al.*, 2011; Eilken and Adams, 2010; Fantin *et al.*, 2010) (Figure I.6).

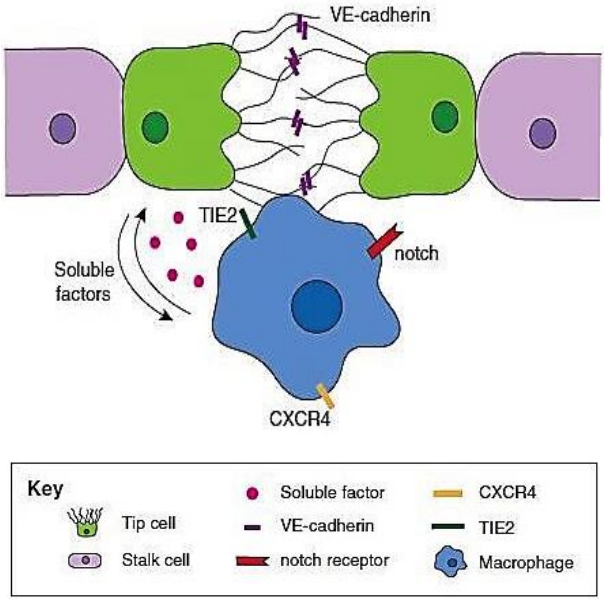

Figure I.6 - Schematic illustration of anastomosis process, during tip cell fusion. Formation of new connections between growing vessels is facilitated by vessel interactions with macrophages (blue) that can act as bridge cells that promote filopodia contact between tip cells (green). Upon contact, adhesion junctions are formed by VE-cadherin, first at the tips of filopodia and later along the extending interface of the contacting cells. Figure from Geudens and Gerhardt (2011).

2.8. Vessel Maturation

Following the initial step of sprouting angiogenesis the newly formed blood vessels must undergo maturation in order to become functional. The process of maturation involves the recruitment of mural cells (pericytes and vSMCs), as well as the generation and deposition of basement membrane and ECM, that will be required for the subsequent remodeling events necessary for the formation of a hierarchically branched network perfectly adapted to local tissue needs. Four distinct molecular pathways are known to be involved in the regulation of this process:

(1) The platelet-derived growth factor (PDGF) B and its receptor (PDGFR)-β;
(2) The sphingosine 1-phosphate (S1P) signaling via its endothelial cell-expressed guanine-nucleotide-binding protein (G protein)-coupled receptor, S1P receptor 1 (S1PR1; also known as EDG1);
(3) The signaling pathway mediated by angiopoietin-1 and its receptor (ANGPT1-Tie2);
(4) The transforming growth factor (TGF)-β (Potente *et al.*, 2011; Jain, 2003).

Endothelial PDGFB activates the receptor PDGFR-β, expressed by mural cells, promoting the recruitment, migration and proliferation of mural cells to nascent vessels. On the other hand TGF-β stimulates mural cell differentiation from mesenchymal cells, their proliferation and migration, but also the production of extracellular matrix. S1PR1 signaling also controls the interaction between endothelial cells and mural cells. S1P from endothelial cells binds to S1PR1, induces cytoskeletal, adhesive and junctional changes, and affects cell migration, proliferation and survival. Lastly, ANGPT1 produced by mural cells, activates its endothelial receptor and the signaling cascade downstream, which is responsible for vessel stabilization, as well as pericyte recruitment and adhesion, that promotes leakage resistance in maturating blood vessels (Potente *et al.*, 2011; Jain, 2003). Whereas

immature capillaries are supported by pericytes, vSMCs are recruited mostly to larger diameter vessels, such as arteries and veins, that are separated from the endothelium by a basement membrane layer (Potente *et al.*, 2011). Importantly, this process can be inverted in response to pro-angiogenic signals, such as VEGF-A or ANGPT2, which promote mural cell detachment and vessel destabilization, thus allowing further rounds of vascular remodeling (Herbert and Stainier, 2011).

2.9. Endothelial cell motility

Migration of endothelial cells is essential for the formation of new blood vessels in the context of physiological and pathological angiogenesis. During angiogenesis, the formation of vascular network from pre-existing blood vessels depends on the collectively migration that shows similar characteristics to individually migration of cells. The biological process can be dependent on both types of migration or one cell type can migrate in both ways depending on the context of migration. In both cases of migration, cells must be polarized and their movement can be random or directional, following a defined motility cycle with typical features (Michaelis, 2014). Thus, cells should acquire an asymmetric morphology with a characteristic leading and trailing edge by actively remodeling their cytoskeleton (Michaelis, 2014; Franco and Li, 2009). One of the main factors regulating endothelial cell migration in sprouting angiogenesis is VEGFA. This morphogen has been shown to promote endothelial migratory behavior and VEGFA gradients modulate tip cell filopodia formation *(Gerhardt et al.*, 2003; Lamalice *et al.*, 2004; Ruhrberg *et al.*, 2002). It is known that filopodia formation involves complex and dynamic rearrangement of actin cytoskeleton networks, and it favors directed cell migration (Mattila and Lappalainen, 2008). However, currently lack a good mechanistic understanding of how VEGFA stimulation regulates endothelial tip cell filopodia formation and tip cell invasion (De Smet *et al.*, 2009; Lamalice *et al.*, 2007).

3. Actin cytoskeleton in motile cells

3.1. Cytoskeleton dynamics

Globular actin (G-actin) is the basic unit of actin filaments. Actin polymerization is controlled by numerous actin binding proteins, which regulate the architecture of actin filaments, forming branched and crosslinked networks (cortex and lamellipodium), parallel bundles (filopodium), or anti-parallel contractile structures (stress fibers) (Blanchoin *et al.*, 2014; Franco and Li, 2009) (Figure I.7). The process of actin polymerization is directly influenced by local intracellular concentrations of ATP-bound G-actin and also by the activity of many G-ABPs. Although actin microfilament turnover involves the regeneration of depleted ATP–actin levels from ADP-actin pools, cell motility also requires the *de novo* biosynthesis of G-actin. Thus, cell motility requires not only the tight temporal coupling of actin dynamics, but also the transcriptional regulation of other structural and regulatory components of the actin microfilament network (Olson and Nordheim, 2010).

The actin cytoskeleton is a highly dynamic structure that is able to respond rapidly to extracellular stimuli through the activation of receptors transforming the received signal into a morphological and/or behavioral change. The dynamic rearrangements of actin filaments generate the physical force necessary for cells to produce filopodia or lamellipodia and to readjust their adhesive contacts to the cellular environment, known as focal adhesions (Olson and Nordheim, 2010; Franco and Li, 2009). In this context, there are a vast number of cellular motile functions triggered by extracellular stimuli that are able to activate different members of the Rho GTPase family (Rho, Rac and Cdc42 subfamilies). Rho GTPases can regulate effector proteins that modulate the polymerization equilibrium of G-actin and F-actin. Enabling G-actin to form complexes with different ABPs, including the nucleating factors profilin, formins and the actin related protein 2/3 complex (ARP2/3 complex) (Olson and Nordheim, 2010).

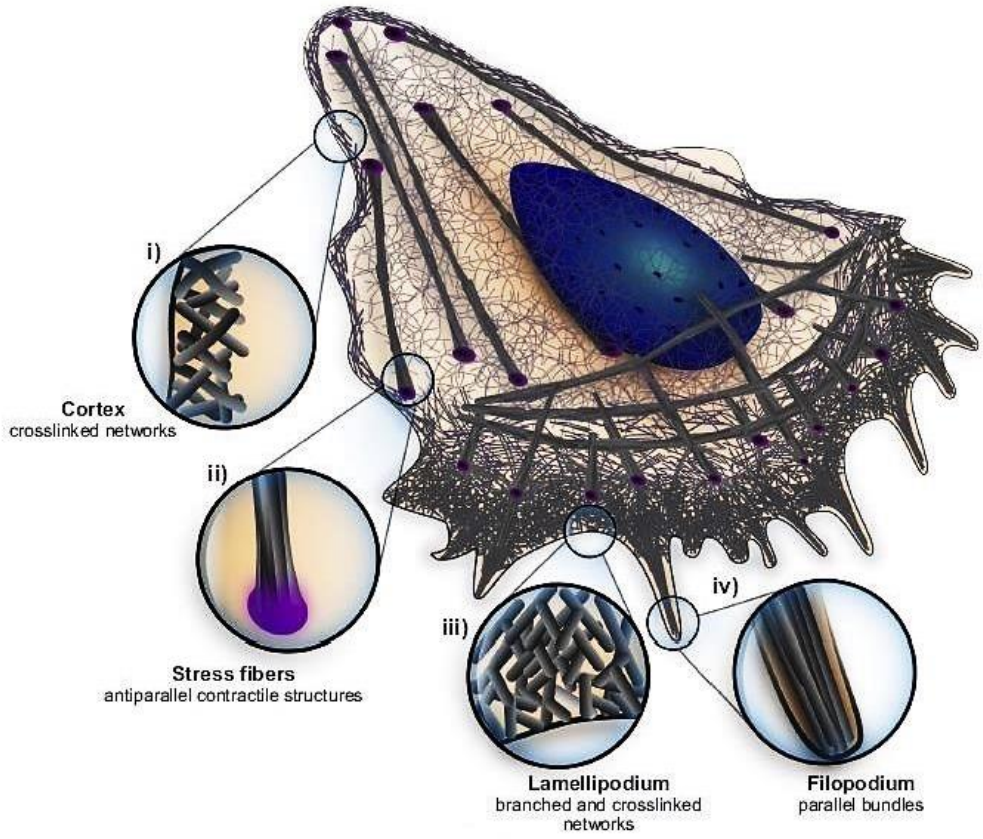

Figure I.7 - Schematic representation of the cell with the different architectures in the motile cell. **i)** the cell cortex; **ii)** an example of a contractile fiber, the stress fiber; **iii)** the lamellpodium; and **iv)** the filopodia. The zoom regions highlight architectural specificities of different regions of the cell. Figure adapted from Blanchoin *et al.* (2014).

3.2. Filopodia and lamellipodia protrusions

Cell motility requires the formation of an actin filament that is nucleated by either formins or the ARP2/3 complex. Following nucleation, cellular protrusions start to form directly via actin assembly or indirectly through myosin contractility of the actin cortex followed by cytoskeleton disassembly (Blanchoin *et al.*, 2014). Thus, when cells initiate migration and acquire an asymmetric polarized morphology, extensive protrusions of the cell membrane driven by the polymerization of actin

filaments start to form at the leading edge towards the external cues, driving cell movement. These protrusions, stabilized by cell adhesions that link the actin cytoskeleton to the underlying ECM proteins, comprise the lamellipodia and finger-like filopodia (Parsons *et al.*, 2010), which are intimately connected to the actomyosin cytoskeleton responsible for cell contraction as well as the generation of traction forces on the substrate. While the actomyosin cytoskeleton, together with cellular projections, act as the main drivers of cell motility, the cell cortex ensures the mechanical integrity and the correct movement of the cell as a whole (Blanchoin *et al.*, 2014) (Figure I.8).

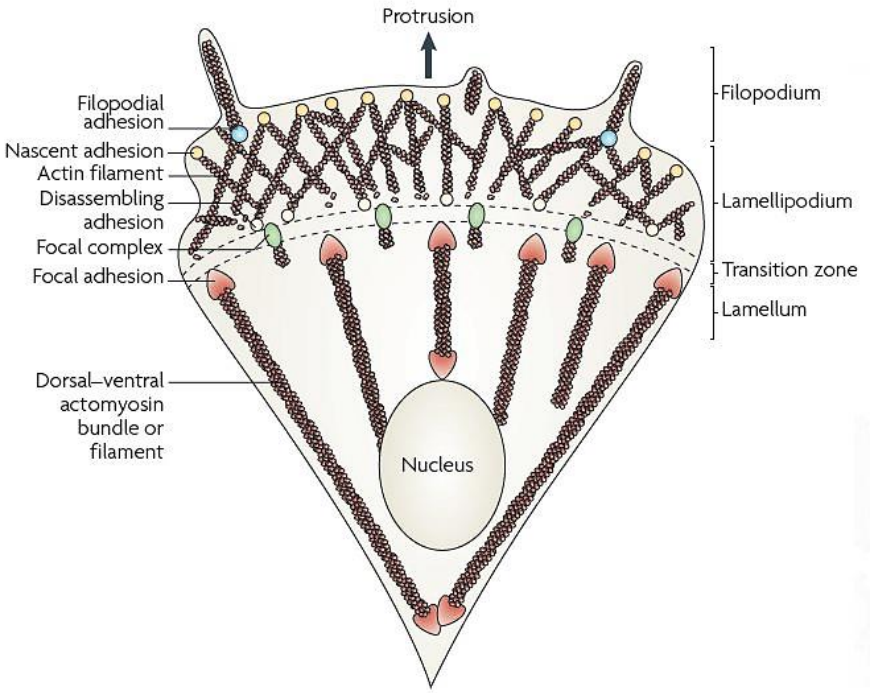

Figure I.8 - Structural elements of a migrating cell. Protrusions comprise large, broad lamellipodia and finger-like filopodia that are driven by the polymerization of actin filaments. Protrusions are then stabilized by adhesions that link the actin cytoskeleton, to the underlying ECM proteins, and actomyosin contraction that generates traction forces on the substrate. Figure adapted from Parsons *et al.* (2010).

Lamellipodia, the pseudopodia-like protrusions, are found at the leading edge of in motile cell and typically form a shallow arc at the most distant point from the cell center and is extended in the direction of travel. However, the movement itself proceeds by periodic protrusion and retraction, with the degree of retraction typically less than that of the protrusion (Heckman and Plummer, 2013). The lamellipodium of the moving cell is a quasi-two-dimensional actin network formed via the assembly filaments, thereby numerous polymerization and nucleation factors play a role in lamellipodia formation (Blanchoin *et al.*, 2014). Two groups of proteins promote actin polymerization: actin nucleators and actin elongators. The major actin nucleator in lamellipodia is the ARP2/3 (complex compound by seven proteins) that promotes the generation of new actin filaments, which branches off the side of a pre-existing filament, together with members of the Wiscott-Aldrich Syndrome protein (WASP) family, such as N-WASP, WASP, and WAVE (Wiskott-Aldrich syndrome protein family verproline-homologous protein (De Smet *et al.*, 2009; Blanchoin *et al.*, 2014). WAVE has been

implicated in lamellipodia and needs Rac1, a membrane-bound GTPase, and lipids to become functional for activating the ARP2/3 complex. This activation results in tight control of ARP2/3 complex-based polymerization at the leading edge of the cell (Blanchoin *et al.*, 2014).

Filopodia are found in many different cell types and display active protrusive, retractile and sweeping motility. This is absolutely essential for their function as cellular sensors that are able to detect soluble cues to define the direction of cell movement (Yang and Svitkina, 2011). These finger-like projections composed of unbranched, bundled actin filaments oriented with their growing ends towards the cell membrane are highly dynamic actin-rich membrane protrusions that extend out from the cell edge (Jacquemet *et al.*, 2015; Blanchoin *et al.*, 2014). Their orientation is due to the presence, in the filopodia tip complex, of formins, such as formin diaphanous-related formin-2 (Dia2) and Ena/VASP proteins, both of which are capable of retaining the growing barbed ends at the cell membrane and enhance filament growth (Blanchoin *et al.*, 2014; Mattila and Lappalainen, 2008). In addition to these regulators, the extension of filopodia driven by the incorporation of actin subunits at the protrusion tips and subsequent release at the rear of the filopodia through a process named treadmilling (Yang and Svitkina, 2011), is controlled by various small GTPases of the Rho family (*i.e.* Rac1 and Cdc42), actin capping proteins, and I-Bar proteins (Insulin receptor substrate IRSp53) (Jacquemet *et al.*, 2015) (Figure I.9). In particular, Cdc42 is involved in the formation of filopodia (Lamalice *et al.*, 2007) and additional studies showed that GTPase Cdc42 is a key molecular player in endothelial cell actin organization, where loss of Cdc42 in endothelial cells, both *in vitro* and *in vivo,* lead to rapid loss of actin organization. Also, loss of Cdc42 during post-natal retinal stages suppresses angiogenic remodeling, filopodia formation and sprouting. As the cytoskeleton anchors junctions, cell adhesion is impaired both between cells and between endothelial cells and cell-extracellular matrix. These findings support that Cdc42 as a key molecular player in sprouting angiogenesis (Barry *et al.*, 2015).

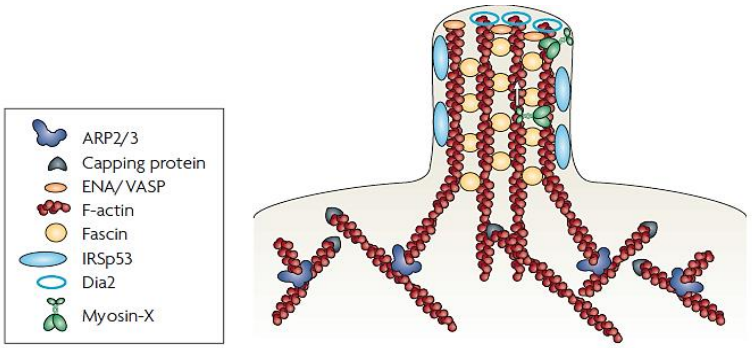

Figure I.9 - Working model for filopodia formation. This model describes functions localizations of key proteins during filopodia formation. Figure adapted from Mattila and Lappalainen (2008).

3.3. Actin/Myosin interactions

Myosins constitute a superfamily of motor proteins that play important roles in several cellular processes that require force and translocation. These molecules can walk along, propel the sliding or produce tension on actin filaments. But for this to happen, energy obtained through the hydrolysis of ATP is required, as well as the availability of myosin catalytic sites with ATPase activity. These

catalytic sites are located in the amino-terminal (head) region of the molecule, and are usually activated when myosin binds to actin. The vast majority of myosins belong to class II. It is important to refer that myosin II molecules resemble their muscle counterparts, with respect to both structure and function, and are also present in all non-muscle eukaryotic cells. In this context, like muscle myosin II, non-muscle myosin II (NMII) molecules are comprised of three pairs of peptides: two heavy chains (MHCs), two regulatory light chains [RLCs, also known as myosin light chain (MLC)] that regulate NMII activity and two light chains (ELCs) that stabilize the heavy chain structure (Vicente-Manzanares *et al.*, 2009) (Figure I.10). Each MHC contains an N-terminal globular motor domain that moves actin as it hydrolyses ATP, as well as a C-terminal tail region that binds to the other MHC, whilst MLC phosphorylation regulates the ATPase activity of MHC (Vicente-Manzanares *et al.*, 2007). NMII can use its actin cross-linking activity and contractile functions, which are regulated by phosphorylation and the ability of NMII to form filaments to regulate the actin cytoskeleton (Vicente-Manzanares et al., 2009).

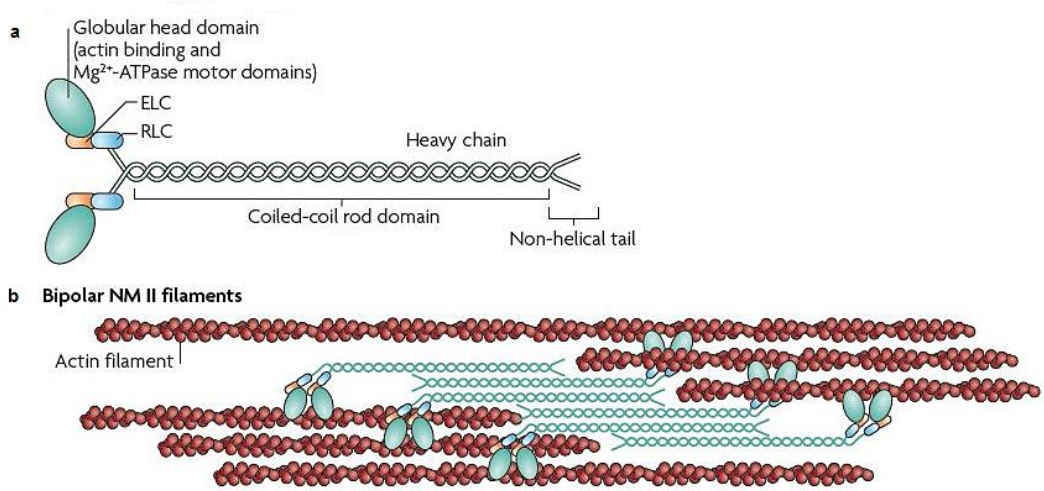

Figure I.10 – Structure of non-muscle myosin II (NM II) and dynamics. a, the subunit and domain structure of myosin, which forms a dimer through interactions between the α-helical coiled-coil rod domains. The globular head domain contains the actin-binding regions and the enzymatic Mg^{2+}-ATPase motor domains. The essential light chains (ELCs) and the regulatory light chains (RLCs) bind to the heavy chains at the lever arms that link the head and rod domains. **b**, NM II molecules assemble into bipolar filaments through interactions between their rod domains. These filaments bind to actin through their head domains and the ATPase activity of the head enables a conformational change that moves actin filaments in an anti-parallel manner. Figure adapted from Vicente-Manzanares *et al.* (2009).

NMII molecules have a fundamental role in cellular reshaping and movement, such as cell adhesion, cell migration, cell contractibility and cell division. Additionally, it is an important end point on which many signaling pathways converge, largely through Rho GTPases. NMII itself is tightly regulated at different levels, including at the level of folding, filament assembly and disassembly, actin binding and ATPase and motor activity (Vicente-Manzanares *et al.*, 2009). There are three different genes in mammalian cells that encode the NMII heavy chain (NMHCII) proteins (NMHCII-A, NMHCII-B and NMHCII-C), myosin heavy chain 9 (*MYH9*), *MYH10 and MYH14.* In contrast, the light chains are

encoded by a different set of genes, which can also undergo alternative splicing, and currently there is no known specificity of light chains for particular NMHCIIs (Vicente-Manzanares *et al.*, 2009).

4. Serum Response Factor (SRF)

4.1. Molecular and biological functions of SRF

The serum response factor (SRF) is an ancient and evolutionarily conserved transcription factor of the MADS-box family (MCM1, Agamous, Deficiens, SRF) and is known to be involved in a wide variety of biological processes (*e.g.* gastrulation, heart, liver and brain development, immune system homeostasis*, etc.*). It is present in most, if not all, species from the animal, plant, and fungi kingdoms and it is expressed in many cell types. Its characteristic name comes from its ability to bind to a serum response element (SRE) site located in the promotor of immediate early transcription factors (Miano *et al.*, 2007). Homodimeric SRF binds with high affinity and specificity to the core palindromic $CC(A/T)_6GG$ DNA sequence of the SRE, called the CArG box, which is common to all SRF-target genes and is responsible for promoting the transcription of numerous target genes involved on distinct signaling cascades (Olson and Nordheim, 2010; Miano *et al.*, 2007).

SRF binding motifs have been identified in the regulatory regions of multiple genes and are known to regulate several processes, such as cell growth, migration, cytoskeletal organization/contractility, energy metabolism and myogenesis (Sun *et al.*, 2006). This transcription factor is seen as the master regulator of genes encoding actin and other contractile proteins, important for the cell cytoskeleton. It is also considered as the major regulator of cytoskeletal protein expression (Franco *et al.*, 2008). There are, nevertheless, functions of SRF that go beyond this transcriptional control of cytoskeletal target genes. SRF can also regulate the transcription of genes involved in cell proliferation and survival (Olson and Nordheim, 2010).

SRF activation occurs mainly through mitogen activated protein kinase (MAPK) or via Rho GTPases/actin dynamics signaling pathways, both converging on the nucleus to induce the transcription of SRF-target genes (Miano *et al.*, 2007; Posern *et al.*, 2002). Through its direct association with the promoter region of target genes, SRF can control the recruitment of several cofactors. Thus, depending on this two signaling inputs, two different cofactors can be recruited to the transcriptional complex:

(1) The ternary complex factor (TCF) subclass of E twenty-six (Ets)-type cofactors (Elk-1, Net and Sap-1);

(2) The myocardin family of coactivators (myocardin-related transcription factors; MRTF-A, MRTF-B, and myocardin itself).

These two type of cofactors have mutually exclusive interactions with SRF and enable it to directly regulate the expression of different sets of target genes (Olson and Nordheim, 2010; Buchwalter *et al.*, 2004). While MRTFs specifically bind to G-actin and respond to fluctuations in its concentration induced by the activity of Rho GTPases, TCF activity is controlled by Ras-MAPK signaling (Ras-Raf-

MEK-ERK signaling) (Clark and Graves, 2014; Esnault *et al.*, 2014) (Figure I.11). Studies performed around the role of the SRF network in the fibroblast by serum response demonstrate a critical role for MRTF signaling. The similarity of MRTF and SRF inactivation phenotypes highly suggest that MRTFs act solely through SRF, in contrast to TCFs that can act redundantly with other Ets proteins, independently of SRF (Esnault *et al.*, 2014).

In addition to TCFs and MRTFs, several other transcription factors have been implicated in SRF regulation, acting as positive and negative SRF cofactors. Although the identities of many proteins involved in SRF regulation are not yet known, it is necessary to learn more about how different signals and cofactors combine to enable the differential transcriptional activity of SRF in different cell types (Posern and Treisman, 2006).

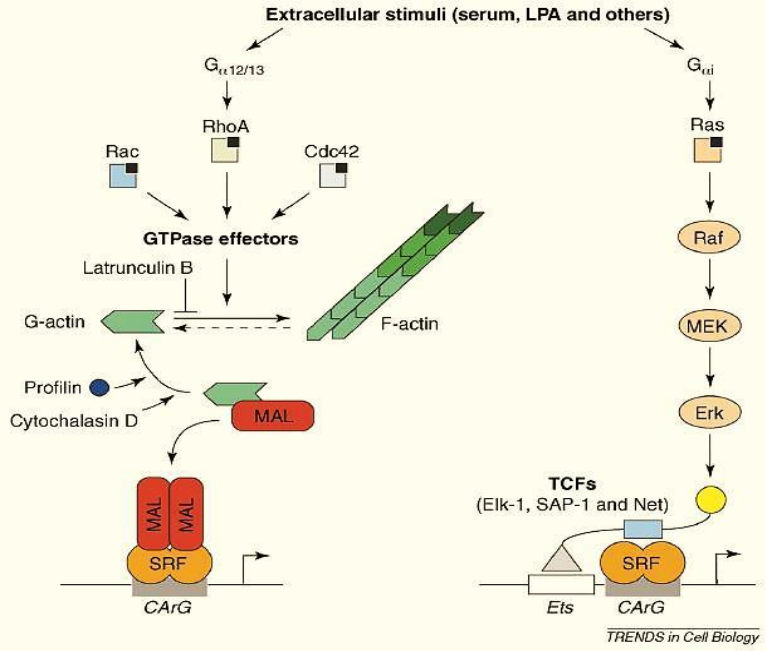

Figure I.11 - Model illustrating the two main pathways regulating SRF activity. Stimulation activates both Rho GTPases-dependent (left) and Ras/MAPK-dependent (right) signaling. Activation of the MAP kinase pathway (right) through Ras, Raf, MEK and ERK phosphorylates TCFs, which bind to their own Ets DNA recognition site and activate SRF. Signaling through Rho family GTPases and the actin treadmilling cycle (left) results in the dissociation of MAL from actin, which then binds and activates SRF. Figure adapted from Posern and Treisman (2006).

4.2. Actin-MRTF-SRF signaling

While myocardin, the founding member of the MRTF family, is expressed specifically in cardiac muscle and smooth muscle cells, the MRTF family members of SRF cofactors, MRTF-A (also called MAL, MKL1 or BSAC) and MRTF-B (also called MKL2 or MAL16), have widespread expression patterns (Olson and Nordheim, 2010; Posern and Treisman, 2006). Although MRTF-A and MRTF-B have distinct functions and/or targets in specific cells, other authors proposed an alternative view arguing that these two proteins are functionally redundant since the knockout of either MRTF-A or MRTF-B reduces the total MRTF activity below a functional threshold (Posern and Treisman, 2006).

In general terms, cytoplasmic concentration of G-actin is reflected by the concentration of MRTFs. When the rate of actin polymerization is reduced, MRTFs form a complex with G-actin (inactive state) and remain in the cytoplasm. The amino termini of MRTFs contain three RPEL domains (conserved N-terminal region containing three RPEL motifs), which form a stable complex with monomeric G-actin, allowing the sequestration of MRTFs in the cytoplasm (Olson and Nordheim, 2010; Wang et al., 2003). However, when cells receive extracellular stimuli stimulating F-actin polymerization, this leads to the release of MRTFs from the G-actin-complex (active state), and to their nuclear import. In the nucleus MRTFs binds to SRF, resulting in the activation of SRF-dependent transcription (Figure I.11). Notably, nuclear G-actin also facilitates the nuclear export of MRTF and prevents activation of SRF target genes. Through this mechanism, the actin–MRTF–SRF circuit links gene expression to actin assembly and disassembly (Olson and Nordheim, 2010; Miralles *et al.*, 2003). Although these regulatory mechanisms have been thoroughly described in muscle cells and cultured fibroblasts, the processes underlying the regulation of the actin–MRTF–SRF circuit in endothelial cells remain poorly understood (Olson and Nordheim, 2010).

4.3. SRF function in sprouting angiogenesis

As previously described, angiogenesis is essential for organ development and function in both physiological and disease contexts. Chai and his colleagues showed that SRF is a downstream mediator of VEGF signaling in endothelial cells and that SRF is required for VEGF-induced endothelial cell migration, proliferation, and actin cytoskeleton rearrangements (Chai *et al.*, 2004). In addition, other studies using a transgenic mouse line Tie1-Cre showed not only that SRF expression is restricted to ECs resident in small vessels of the mouse embryo, but also that its presence is particularly important for the expression of β-actin and VE-cadherin in these cells. Furthermore, *SRF* inactivation in embryonic endothelial cells leads to a decrease in the number of branching points, alterations in tip cell morphology and filopodia, and the disruption of endothelial cell junctions, leading to embryonic death. Therefore, SRF has a crucial role in sprouting angiogenesis and in the maintenance of small vessel integrity (Franco and Li, 2009; Franco *et al.*, 2008). Induced endothelial *SRF* deletion at different time points in post-natal mice showed dramatic growth retardation, decreased viability, inducing systemic hypovascularization and severe retinal angiopathies (Franco *et al.*, 2013; Weinl *et al.*, 2013).

During both embryonic and post-natal angiogenesis, SRF is strongly expressed by endothelial cells at the sprouting front, both in tip and stalk cells. SRF is essential for filopodia formation and tip cell invasion downstream of VEGF signaling (Franco and Li, 2009; Franco *et al.*, 2008). Notably, Weinl and colleagues also showed that double-KO mice with endothelial cell-specific MRTF-B deletion ($Mrtfa^{-/-}Mrtfb^{iECKO}$ mice) and Srf^{iECKO} mice have a highly overlapping phenotypic characteristics phenotype, suggesting that MRTFs are the relevant endothelial cell SRF cofactors *in vivo* ensuring appropriate retinal angiogenesis (Weinl *et al.*, 2013). Mechanistically, VEGF-A signaling activates G-actin–dependent MRTF-A translocation from the cytoplasm to the nucleus and MRTF/SRF transcriptional activity. MRTF/SRF signaling output in endothelial cells promotes cytoskeleton and junctional reorganization for efficient endothelial sprouting (Franco *et al.*, 2013; Weinl *et al.*, 2013).

Interestingly, SRF expression is increased in human tumor endothelium, and, curiously *SRF* deletion in mouse tumor models impairs tumor angiogenesis (Franco *et al.*, 2013). MRTF/SRF signaling, in this context, controls the expression of *MYL9*. Decreased expression of *MYL9* is sufficient to impair endothelial cell migration (Franco *et al.*, 2013). Given the specific and central function the MRTF/SRF is a potential target for pathological angiogenesis.

5. Working Models for studying vascular development

Several different *in vitro* models and techniques are predominantly used to characterize the signaling pathways controlling angiogenesis and to identify new therapeutic targets. These approaches include wound healing/scratch wound cell migration assays, EC proliferation assays, network formation assays in Matrigel and three-dimensional angiogenesis assays, such as the aortic ring assay and assays of capillary-like structures formation in fibrin or collagen. However, these techniques have some limitations, most they focus on isolated steps of angiogenesis and are affected by artificial experimental settings, such as lack of blood flow, different origins of ECs and different cell culture media (Pitulescu *et al.*, 2010). In this context, most of angiogenic studies are also performed through *in vivo* assays, such as zebrafish embryos, post-natal mouse retinas and various tumors models.

5.1. Mouse retinal model

The post-natal retinal model has contributed significantly to understanding the mechanisms of angiogenic sprouting (Geudens and Gerhardt, 2011). As in other tissues, retina blood vessels undergo extensive changes during development. Efficient analyses may be performed in a single system, the retina, at various stages of post-natal life. Also, the retina is an excellent system for certain models of pathological angiogenesis. Using the mouse retinal model allows the analysis of angiogenesis in newborn, young and adult mutant mice, drug-treated animals or disease models with pathological vascularization (Pitulescu et al., 2010). In addition, retinas are ideal structures to visualize using whole-mount immunostaining and in-situ hybridization techniques, coupled with high resolution three-dimensional imaging by confocal laser scanning microscopy (Gerhardt et al., 2003). Thus, with this developmental model of angiogenesis the stereotypical vascular pattern of the early postnatal mouse retina may be studied in a well-defined sequence of events. Before birth, the hyaloid vasculature supplies the inner eye and lens with nutrients and oxygen. In contrast, after birth, these hyaloid vessels start to regress and a new vascular plexus forms rapidly. In the first days, a primitive vascular plexus will be formed by sprouting, endothelial cell proliferation and migration, following later by remodeling and maturation into a hierarchical vascular tree of arteries, veins and interconnecting capillaries (Pitulescu et al., 2010). Therefore, from birth until postnatal day 7 (P7), the endothelial network extends gradually from the center of the retina towards the periphery. After this initial two-dimensional vascular growth period, sprouting into the deeper retinal layers begins, and within the next 1–2 weeks, depending on the mouse strain, deep and intermediate vascular plexuses are completely formed (Pitulescu *et al.*, 2010; Gerhardt *et al.*, 2003) (Figure I.12).

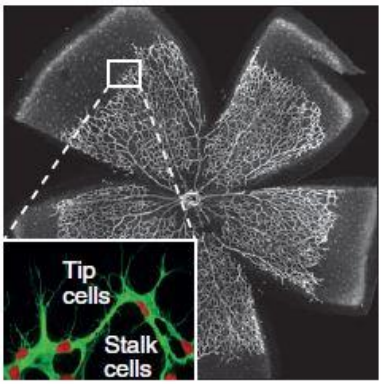

Figure I.12 - Schematic illustration of a growing sprout in mouse retina. Vessel networks and sprouts in mouse retinal model system at post-natal day (P) 5. Inset shows higher magnification of sprouting front showing tip cells with filopodia and stalk cells. Red shows the endothelial nuclei (Erg), green shows the Isolectin-B4 that labeled the endothelial cells. Figure adapted from Geudens and Gerhardt (2011).

5.2. Spheroid sprouting assay

Between classical angiogenesis models, the spheroid sprouting assay consists of the self-aggregation of endothelial cells embedded in a 3D matrix leading to endothelial cell sprouting and invasion into the surrounding matrix. This approached in later situation perfectly reproduces the formation of capillaries from pre-existing vessels and has numerous advantages. As a result, this 3D-gel-embedded EC spheroid model has gained broad acceptance. This technique provides a better mimic of the *in vivo* environment than classical 2D-cultures, is rapid and easy to use, takes into account different cell properties involved in angiogenesis (e.g., cell proliferation, migration, invasion and survival), lacks inflammatory complications and thus facilitates the investigation of cellular and molecular mechanisms underlying angiogenesis. Furthermore, defined experimental conditions can easily be achieved to facilitate screens for pro- or anti-angiogenic agents and to evaluate the impact of biochemical and/or physical barriers on cell invasion (Blacher *et al.*, 2014).

6. Aims

As previously described, SRF is important for post-natal angiogenesis. SRF deletion affects new blood vessel formation (Franco *et al.*, 2013). Also, endothelial tip cells lacking SRF have fewer filopodia and drastically decreased propensity to invade and migrate towards VEGF-A gradient (Franco *et al.*, 2013; Weinl *et al.*, 2013). In this context, the main goal of this master thesis project was to find cytoskeletal proteins involved in the regulation of endothelial tip cells downstream of SRF signaling during sprouting angiogenesis. Achieving this aim will be important for improving and implementing new and more effective therapeutic approaches targeting to inhibit pathological vascularization.

Claudios Franco's Lab defined a core of endothelium SRF-target genes using Affimetrix microarray sequencing. These genes are likely involved in the regulation of actin dynamics, filopodia formation and endothelial cell migration during angiogenesis. Thus, my specific goal was to identify which genes downstream of SRF transcriptional regulation are required for efficient cell migration. Towards this goal, I had a specific approach involving the specific tasks:

- Validation of expression levels in candidate genes
- Functional validation of positive candidates genes
- Rescue of SRF-Knockdown phenotype

II. MATERIALS AND METHODS

1. Mice breeding and genotyping

During this project we used the LifeAct-GFP (Riedl *et al.*, 2010) mouse line. The LifeAct-GFP mouse expresses an actin-binding protein fused to eGFP that labels filamentous actin specifically.

Mouse genomic DNA isolation was performed using a NaOH extraction protocol from samples of ear/tail. The tails/ears snips were collected into an 1.5mL eppendorf tube, 200µL of 25mM NaOH/0.2mM EDTA was added and the samples were incubated 1h at 98ºC in a Dry Block Thermostat (Grant Instruments, Ltd). After the incubation tubes were vortexed vigorously and the samples were neutralized with 30µL of 100mM Tris-HCl (pH8), following a centrifugation at maximum speed for 10min. Samples were then kept at 4˚C until DNA amplification and further processing.

Mice were genotyped by PCR with NZYTaq 2x Colourless Master Mix (Nzytech, Lda), following a standard protocol of 20 µL (total volume per reaction). 1.5µL of isolated DNA was mixed with 10µL of NZYTaq 2x Colourless Master Mix, 1µL of 4µM primers pool (forward+reverse) (Table II.1) and 7.5µL Milli-Q RNAse/DNAse free water. The PCR reaction was performed using the MyCycler™ Thermal Cycler™ (Bio-Rad Laboratories) following a specific set of parameters (shown in Table II.2). Following PCR amplification, 3.3µL of 6x NZYDNA loading dye (Nzytech, Lda) were added to each PCR product and a electrophoresis in a 2% agarose (Nzytech, Lda) gel in TBE buffer (1M Tris, 1M boric acid, 0.02M EDTA in H_2O) was conducted. 5µL of DNA ladder GeneRuler 1kb Plus (Thermo Scientific) were used as a ladder during this protocol and the 2% agarose gel was stained with GreenSafe (Nzytech) and analyzed in a Chemidoc equipment (Bio-Rad Laboratories).

All animals were fed freely and housed in SPF facilities. Animal experiments were approved by the Animal Ethics Committee of Instituto de Medicina Molecular (iMM Lisboa) and according to National Regulations.

Table II.1 - Primers used for genotyping PCR. Representative table of primers sequence used in genotyping PCR with respective orientation.

Strain	Primers Name	Primers Sequence (5'→3')	Orientation
Rosa26-mTmG	R26mTmG - C	CTC TGC TGC CTC CTG GCT TCT	Forward
	R26mTmG - WT	CGA GGC GGA TCA CAA GCA ATA	Reverse
	R26mTmG - TG	TCA ATG GGC GGG GGT CGT T	Reverse
SRF floxed	SRF - F	CTG TAA GGG ATG GAA GCA GA	Forward
	SRF - R	TAA GGA CAG TGA GGT CCC TA	Reverse
	SRF - FL	TTC GGA ACT GCC GGG CAC TAA A	Reverse
LifeAct-GFP	LifeAct - F	GCA CGA CTT CTT CAA GTC CGC CAT GCC	Forward
	LifeAct - R	GCG GAT CTT GAA GTT CAC CTT GAT GCC	Reverse
CRE (Prox1-iCRE)	CRE - F	CTT CTG TCC GTT TGC CGG TCG TGG	Forward
	CRE- R	TTT TGC ACG TTC ACC GGC ATC AAC G	Reverse
PDGFB-iCRE	Pb-iCRE - F	GCC GCC GGG ATC ACT CTC G	Forward
	Pb-iCRE - R	CCA GCC GCC GTC GCA ACT C	Reverse

Table II.2 - Genotyping PCR program. Representative table of PCR conditions (temperature, time and cycles) for genotyping.

Cycle step	Temperature	Time	Cycles
Initial denaturation	95˚C	120sec	1
Denaturation	95˚C	30sec	30
Annealing	60˚C	30sec	
Extension	72˚C	60sec	
Final Extension	72˚C	10min	1

2. Culture of Human Umbilical Vein Endothelial Cells (HUVECs)

HUVECs (C2519A, Lonza) were routinely cultured, following the manufacturer's manual, in filter-cap T75 flasks Nunclon™Δ surface treatment (VWR international, LLC) with complete culture medium EGM™-2 BulletKit™ (CC-3162, Lonza) without gentamicin sulfate amphotericin-B antibiotic (GA) and were incubated at 37˚C and 5% CO_2 to ensure a stable environment for optimal cell growth. All experiments were done with HUVECs between passages 2 to 6.

Normal passaging of cells was performed from 1 flask at 80-90% of confluence splitted into 4-5 flasks. Cells were washed twice with sterile 6mL of PBS (For 500mL of PBS 10x: 40g NaCl,1 g KCl, 7.2g Na_2HPO_4, 1.2g KH_2PO_4, pH7.4). After washes, 3mL of trypsin/EDTA was added and the cells were incubated for 2-3min at 37ºC (cell detachment was monitored using a microscope, Leica DMIL LED Fluo). When 95% of cells detached, 3mL of medium was added to each flask in order to inhibit the activity of trypsin/EDTA and the medium with the detached cells was collected into a falcon tube. To maximize the amount of cells collected, 3mL of medium was used to wash all flasks and the volume was combined to the previously used falcon tube. Cells were then collected and centrifuged at 700rpm for 5min. When passing HUVECs for experiments, cells were re-suspended in 5mL of medium and the cell concentration counted with a Neubauer Chamber Cell Counting (Hirschmann® EM Techcolor) for 150 000 cells/mL. Half of the total volume was distributed per each well that previously had the other half of warm medium. The flasks or plates were then mixed and placed in the incubator.

3. VEGF induction in HUVECs

VEGF induction was performed for gene and protein expressions assays after siRNA experiments (described in II.4). For this induction, the culture medium was replaced with serum free medium (SFM), EBM™-2-growth factor-free medium (CC-3156, Lonza), supplemented with 0.2% Fetal Bovine Serum (FBS, gibco® by life techonologies) and incubated overnight (ON) at 37ºC. In the next day, cells were then left untreated or stimulated with VEGFA165 (50 ng/ml; PeproTech) and after 30min (in the case of RNA extraction) or 2h (in the case of protein), the medium was removed and the RNA or protein was extracted according to standard procedures.

4. siRNA experiments

In order to silence the expression of target genes, a set of ON-TARGET siRNAs against human *SRF*, *MKL1*, *MKL2, MYH9, FLNA, TPM2, TAGLN2, TPM1, LIMA1, TPM4, ACTR3, MICAL2* and a control siRNA was used. All siRNAs were purchased from Dharmacon™ (siRNA sequences catalog number in Table II.3). HUVECs were seeded the day before in order to reach a 60-70% confluence before transfection. Cells were then transfected with a 25nM specific siRNA using the DharmaFECT 1 transfection reagent (Dharmacon™, GE Healthcare) following the Dharmacon™ siRNA Transfection Protocol. 24h after transfection, the culture medium was replaced for fresh complete culturing medium.

For protein extraction and immunostaining, cells were cultured 92h post-transfection, and for RNA extraction cells stayed in culture at least 48h until reaching maximal confluence.

Table II.3 - siRNA sequences used in siRNA experiments. Representative table ON-TARGET siRNA target sequences catalog number (-1, -2 and - 3 represents the 3 siRNA for each candidate gene)

siRNA name	siRNA target sequences catalog number
siControl	D-001810-01
siSRF	J-009800-08-0002
siMKL1	L-015434-00-0005
siMKL2	L-019279-00-0005
siMYH9-1	J-007668-05
siMYH9-2	J-007668-06
siMYH9-3	J-007668-07
siFLNA-1	J-012579-05
siFLNA-2	J-012579-06
siFLNA-3	J-012579-07
siTPM1-1	J-017837-05
siTPM1-2	J-017837-06
siTPM1-3	J-017837-07
siTPM2-1	J-012657-05
siTPM2-2	J-012657-06
siTPM2-3	J-012657-07
siTPM4-1	J-019753-05
siTPM4-2	J-019753-06
siTPM4-3	J-019753-07
siTAGLN2-1	J-011468-05
siTAGLN2-2	J-011468-06
siTAGLN2-3	J-011468-07
siLIMA1-1	J-010663-09
siLIMA1-2	J-010663-17
siLIMA1-3	J-010663-18
siACTR3-1	J-012077-06
siACTR3-1	J-012077-07
siACTR3-1	J-012077-08
siMICAL2-1	J-010189-05
siMICAL2-2	J-010189-06
siMICAL2-3	J-010189-07

5. Overexpression of MIIA-GFP in SRF depleted HUVECs

To assess whether the overexpression of MIIA-GFP was able to rescue the phenotype of SRF depleted HUVECs, we transfected HUVECs with CMV-GFP-NMHC II-A (MYH9 human) plasmid (Addgene plasmid #11347), carried out by Lipofectamine® LTX & PLUS™ reagent (Invitrogen™ by Life Technologies™), after 24h of siRNA transfection (described in II.4). This experiment was performed only in 24-well plates, with a few modifications of the manufacturer's protocol and the volumes were adjusted to avoid pipetting errors. First, mix 1 and mix 2 were prepared as described in Table II.2. Then, mix 3 (Table II.3) was done and incubated for 15min at room temperature (RT). After that, in order to form DNA-Lipofectamine® LTX complexes, a final mix, mix 4, was made (Table II.2) and incubated 25min at RT. Finally, we added 400µL of warm complete culture medium. We removed the medium of plate and the transfection mixture was then added to the well-plate and 24h later, the medium was replaced for complete culture medium.

Table II.4 - Lipofectamine® LTX DNA Transfection Protocol. Representative table of the DNA and reagents per well used in 24-well plate.

Mixes per well	PLUS™ reagent	Lipofectamine® LTX reagent	Plasmid DNA (100ng/µL)	SFM
Mix 1	2.5µL	-	-	250µL
Mix 2	-	1.5µL	-	250µL
Mix 3	30µL from mix1	-	3µL	70µL
Mix 4	25µL from mix 3	25µL from mix 2	-	-

6. Gene expression assays

RNA extraction from 6 and 12-well plates from seeded HUVECs was performed using the RNeasy® Mini Kit (Qiagen) as described by the manufacturer's protocol. RNA was eluted in a final volume of 30µL, quantified using NanoDrop 1000 (Thermo Scientific) and adjusted equally, followed by DNase digestion and reverse transcription. DNase I digestion that digests a single- and double-stranded DNA was performed using the DNase I, RNase-free (Thermo Scientific) with 1µg of RNA, following the manufacturer's protocol. cDNA synthesis from RNA was performed using High Capacity RNA-to-cDNA Kit (Applied Biosystems®) with 1µg of RNA according to the manufacturer protocol using the MyCycler™ Thermal Cycler™ (Bio-Rad Laboratories). The cDNA samples were diluted 25x for the subsequent quantitative real-time PCR (qPCR) reactions.

Quantitative real-time PCR was performed using a 7500 Fast Real-Time PCR System (7500 software v2.0.6) (Applied Biosystems®) with Power SYBR® Green PCR Master Mix (Applied Biosystems®) following the standard program of this Real-Time PCR System. In this experiment, 5µL of cDNA sample was combined with 15µL qRT-PCR mixture [10µL of Power SYBR® Green PCR Master Mix, 0.5µL of 4µM primers pool (forward+reverse) (Table II.5); and 4.5µL Milli-Q RNAse/DNAse free water] in MicroAmp® Fast Optical 96-well Reaction Plate (Applied Biosystems®). The expression levels were normalized to GAPDH (a housekeeping gene) and $2^{-\Delta\Delta T}$ method was used to analyze relative changes in gene expression.

Table II.5 - Primers used in qPCR. Representative table of primers sequence used in qPCR

Primer Name	Forward Sequence (5'→3')	Reverse Sequence (5'→3')
SRF	GCC GCG TGA AGA TCA AGA TG	GTC AGC GTG GAC AGC TCA TA
MKL1	CAG AAC AGC ACC TCA CTG ACT G	CAG GCA GTG ATC GCA ACT TCA G
MKL2	CAG AGT GTC GTC TCG CAG TT	GTC TGA GGT ACA GTT GGG GC
FLNA	CAA CAA GTT CAC TGT GGA GAC CA	TGT AGG TGC CAG CCT CAT AAG G
ACTR3	CTG TAG ATG CCC GGC TGA AA	TAT CGC TGC ATG TGG TGT GT
TPM1	ATGCCATTCTTGCCCAGGAG	GGTGCGCCTATGACACTTCT
TPM2	CCA GGC GGA CAA GTA TTC CA	ACT TTG CCA CAG ACC TCT CG
TPM4	GGG CCA TGA AGG ATG AGG AG	AGG ATG ACC AGC TTA CGA GC
FILIP1	CAC CGA GAT GCC ATT CTT GC	GCG CCG GTA GGT TTC TTT CT
LIMA1	AAA CAC AGA TGC TTC GGG CA	CCA CTT GCA CTT CGG CTT TG
MICAL2	AAC AAA CGG AGA CGG AAG GG	AGC TGA TTC GCC ATG GAC TT
MYH9	GGA GTA TGA TGC AAG ACC GA	CGT ACG CCA GAT ACT GGA TG
MYL9	ACA TGA TTG ACC AGA ACC GTG A	CCC TCC AGG TAT TCG TCT GTG
TAGLN2	ATG GGC TCT TCT CTG GGG AT	TTG GTG CCC ATC TGT AAC CC
PALLD	GCT AGG TGC TGA CAG TGC AA	ACC ATC CAG AGG ACT CCC TAC
NEXN	GAG GAG GAA CGA AAA CGC AG	TGA TGC TGA TTC AGT TCC CGT A
GAPDH	GTC AAG GCT GAG AAC GGG AA	TGG ACT CCA CGA CGT ACT CA

7. Protein extraction and Western Blotting

7.1. Protein lysis and sample processing

For Western blot analysis, HUVECs in 6-well plates were lysed with 100uL of RIPA buffer (50mM Tris/HCl pH7.5, 1% NP-40,150mM NaCl, 0.5% Sodium Deoxycholate, 0.1% SDS, in H_2O) supplemented with Phosphatase and protease inhibitors cocktail (PIs) and EDTA (1:100, 10085973 Fisher Scientific). Then, using a cell scrapper, the adherent cells of the dish were detached and the cell lysates were transferred into an ice-cold 1.5mL eppendorf tube. All steps were performed in ice. Then, these cell lysates were centrifuged for 10min at maximum speed (4˚C) and the supernatants were transferred into a new ice-cold 1.5mL eppendorf tube. The protein concentration of the samples was quantified using the BCA protein assay kit (Pierce) following the instructions recommended by the manufacturer. The Multimode microplate reader, Infinite M200 (Tecan), was used for spectrophotometric measurement of protein with i-control™ software. Protein extract samples were adjusted equally until 25µL and diluted in 1:10 of 2-Mercaptoethanol (M6250, Sigma-Aldrich), 1:4 of 4x Laemmli Sample Buffer (161-0747, Bio-Rad Laboratories) and H_2O until the final volume (35µL). Samples were incubated at 70ºC in a Dry Block Thermostat (Grant Instruments, Ltd) for 10min and spinned for 30sec to recover all the volume.

7.2. Protein electrophoresis and membrane transference

Equal amounts of protein were separated on a 4–15% Mini-PROTEAN® TGX™ Gels (456-1084, BioRad) along with 5µL PageRuler Plus Prestained Protein Ladder (Thermo Scientific). Samples were runned first for 5min at 50V and then for 1-2h at 150V, until the end of running, with 1x SDS-PAGE running buffer (10x SDS-PAGE: 250mM Tris, 1.92M glycine, 1%SDS, pH8.3). When electrophoresis was finished, a pretreatment of the gels in 20% ethanol (prepared in deionized water) for 10min before membrane transference in order to improve the transfer of proteins >150 kDa. Then, the gel was transferred to a nitrocellulose membrane (iBlot™ Transfer Stack regular/mini size, IB3010-01/-02, Invitrogen™) with iBlot™ Dry Blotting System (Invitrogen™), program 3 for 8min. After transfer, blotted membranes were incubated at RT during 1h in blocking buffer containing 3% BSA in Tris buffered saline/ 0.1% Tween 20 (referred as TBS-T); TBS 10x buffer was done with 30.5g Tris (0.5M) and 45g NaCl (1.55M) at pH7.6 in H_2O. After that, membranes were incubated ON at 4ºC with primary antibodies diluted in the blocking buffer (described in II.11, Table II.6). In the following day, membranes were washed 3x (10min each) with TBS-T and incubated for 1h at RT with blocking buffer containing the secondary antibodies horseradish peroxidase (HRP) Conjugated (described in II.11, Table II.7). Upon incubation with secondary antibodies, membranes were washed 3x (10min each) with TBS-T and protein detection was performed by enhanced chemiluminescense (ECL) with ECL™ Western Blotting Detection Reagent (RPN2209, GE Healthcare) following the manufacturer´s protocol. Bands were visualized in a Chemidoc equipment and relative intensities of protein bands were analyzed using the Image Lab 5.1 software, both from Bio-Rad Laboratories. All the results were normalized to Tubulin levels.

8. Scratch-wound assay

The Scratch-wound assay was used during this project in order to study the morphology, as well as the functional migration of *in vitro* cultured HUVECs. The wound was created by scratching a well-plate containing a monolayer of HUVECs, using a 200uL pipette cone, followed by 30min incubation at 37˚C. Then, the culture medium was removed and replaced by fresh complete medium and HUVECs were allowed to migrate. For immunofluorescence staining (described below in section II.9), HUVECs were allowed to migrate during 5h, while through live imaging, the wounded area was monitored using a Spinning Disk Confocal Microscope, Zeiss Cell Observer SD (Carl Zeiss) equipped with the ZEN 2 edition software, for 16h with photos taken every 10min. Results were analyzed using the Fiji software.

9. Immunofluorescence staining of cultured HUVECs in coverslips

For immunostaining of cultured HUVECs, cells at passage 4 were seeded in 24-well plates with coverslips. Coated treatment of coverslips was performed on the day of cell seeding. For coating 300µL of poly-L-lysine 0.01% solution (Sigma-Aldrich) was added to each coverslip following by 15min incubation at 37˚C. After this, the coverslips were rinsed twice in PBS and once in sterile H_2O. Finally,

300µL of gelatin solution 0.2% (Sigma-Aldrich) dissolved in sterile H_2O were added followed by 30min incubation at 37˚C.

After the scratch-wound assay (described in II.8), HUVECs were fixed with 300µL per well of 1% paraformaldehyde (PFA) supplemented with equal concentration of 1M $MgCl_2$ and 1M $CaCl_2$ (1µL:2mL) in PBS for 30min at RT with gentle agitation. Cells were then washed with PBS to remove any remaining PFA and the immunostaining protocol was conducted.

All steps of immunostaining were performed at RT with gentle agitation. First, PBS was removed and HUVECs were blocked and permeabilized 30min with 200µL per well with blocking solution (3% Bovine Serum Albumin (BSA, Nzytech, Lda) in PBS-T (PBS/0.1% Triton™ X-100 (Sigma-Aldrich)). Afterwards cells were incubated with the primary antibodies diluted in blocking solution (described in II.11, Table II.6) for 2h, followed by 3 washes of 15min with PBS-T. After the washes, cells were incubated with the secondary antibodies (described in II.11, Table II.7) for 1h and then washed again as before. After this, 4',6-Diamidino-2-Phenylindole, Dihydrochloride (DAPI, D1306, Molecular Probes™ by life technology) treatment (1:1000, diluted in PBS-T) was performed (200 µL per well) for 5min.

Whole mount of coverslips was performed using Mowiol/DABCO (Sigma-Aldrich). High-resolution three-dimensional rendering of coverslips was acquired with two microscopes, the confocal Laser Point-Scanning Microscope 710 (Zeiss) equipped with the ZEN black 2012 edition software and the motorized inverted widefield fluorescence microscope, Zeiss Axiovert 200M (Carl Zeiss), equipped with the Metamorph software v7.8.0.0. Results were analyzed using the Fiji and Imaris 8.0 software.

10. Eyes extraction and retina isolation for immunoflorescence

Pups were sacrificed by decapitation and eyes were quickly collected using forceps and scissors. Eyes were fixed in a 2% PFA solution diluted in PBS for 5h at 4°C. After fixation, the eyes were washed with PBS to remove any remaining PFA and the retinal dissection protocol was performed.

Retinal dissection was done in a culture glass dish with PBS using a binocular dissecting microscope (Carl Zeiss). Using the forceps, an incision between the cornea and the iris was done and the cornea, iris, sclera, optic nerve, the lens, the vitreous humor and the pigmented retina layer were separated and removed. Finally, the hyaloid vessels were carefully detached using rotating fine movements. We then performed the 4 cuts using micro-scissors in order to separate the retina into four quadrants (Figure II.1).

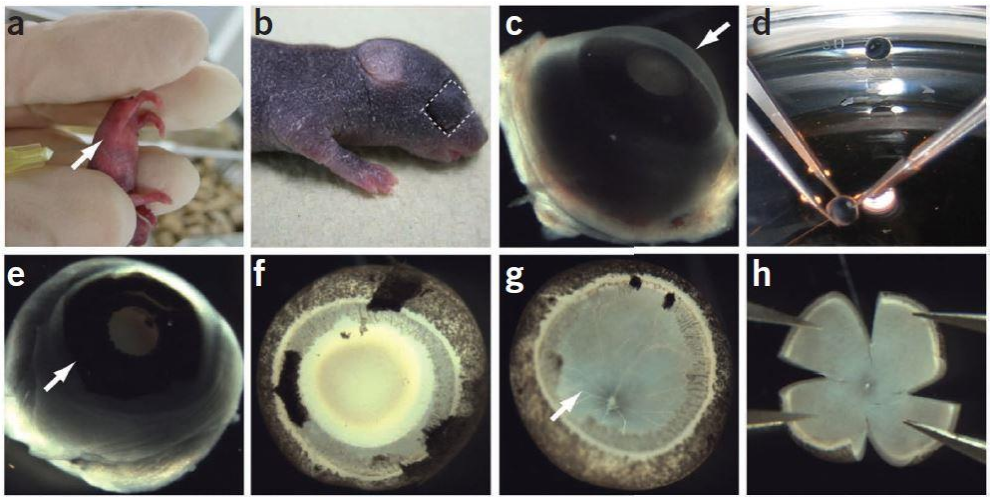

Figure II.1 - Tamoxifen injection, eye and retina dissection. a, Intraperitoneal tamoxifen injection in a P1 mouse pup. **b**, The incision around the eye for eye collection. **c**, Dissected eye, arrow showed the first incision point between cornea and iris. **d**, Overview of cornea dissection. (e) Eyeball without cornea, arrow indicates dissected cornea. **f**, Eye without sclera, choroid, cornea layers, pigmented layers and without some iris. **g**, Dissected eye without a lens, arrow shows hyaloid vessels. (h) Retina with four radial incisions. Figure based from Pitulescu *et al.* (2010).

10.1. Immunofluorescence staining in whole-mount retinas

For staining, retinas were blocked and permeabilized with 200µL of blocking solution (1% Fetal Bovine Serum (FBS, 10270, gibco® by life techonologies), 3% BSA, 0.5% Triton X-100, 0.01% Na deoxycholate, 0.02% Na Azide in PBS) 2h at RT with gentle rocking. Afterwards, retinas were incubated with primary antibodies in appropriated dilutions (described in II.11, Table II.6) in 1:1 Blocking solution: PBS ON at 4°C with gentle rocking (100µL per retina in a round-bottom 2 mL tube). On the next day, retinas were washed 4x30/60min with PBS-T at RT with gentle rocking. After washing, the retinas were incubated with secondary antibodies in appropriated dilutions (described in II.11, Table II.7) at 4ºC ON with gentle rocking. On the following day, retinas were washed 3x30min with PBS-T at RTand finally treated with DAPI for 10min (1:1000, diluted in PBS-T).

Whole mount was performed using VectaShield mounting medium (H-1000, Vector Laboratories). High-resolution three-dimensional rendering of retinas was acquired using a Confocal Laser Point-Scanning Microscope 710 (Carl Zeiss) equipped with the ZEN black 2012 edition software.

11. Antibodies and other molecular probes

In the following tables (Table II.6 and II.7) the primary and secondary antibodies used during this project are shown with the respective dilutions.

Table II.6 - Primary antibodies used and respective information (*dilutions for spheroids).

Primary antibody	Host	Brand	Dilutions for mouse retina	Dilutions for HUVECs	Dilutions for WB
Anti-SRF	Rabbit	Santa Cruz Biotechonology® (sc-13029)	-	1:100	1:500
Anti-MRTF-A	Goat	Santa Cruz Biotechonology® (sc-21558)	-	1:50	-
Anti-Myosin IIA	Rabbit	Sigma-Aldrich™ (M8064)	1:2000	1:200*	1:2000
Anti-p-MLC	Rabbit	Abcam® (ab2480)	-	-	1:2000
Anti-MLC2	Rabbit	Cell Signaling Techonology® (#8505)	-	-	1:1000
Anti-TPM4	Rabbit	Abcam® (ab181085)	-	-	1:2000
Anti- α-TPM	Mouse	Sigma-Aldrich™ (T2780)	-	-	1:2000
Anti-TAGLN2	Rabbit	Sigma-Aldrich™ (HPA001925)	-	-	1:1000
Anti-FLNA	Rabbit	Sigma-Aldrich™ (HPA001115)	-	-	1:2000
Anti- CD31	Goat	R&D systems® (AF3628)	1:400	-	-
Anti-LIMA1	Rabbit	Sigma-Aldrich™ (HPA023871)	-	-	1:2000
Anti-Vinculin	Mouse	Abcam® (ab18058)	-	1:100	-
Anti-actin	Goat	Santa Cruz Biotechonology® (sc-1616)	-	-	1:1000
Anti-α-tubulin	Mouse	Sigma-Aldrich™ (T6199)		-	1:2000
Anti-ZO1	Rabbit	Invitrogen™ (402300)	-	1:100	-

Table II.7 - Secondary antibodies and Phalloidin used and respective information (*dilutions for spheroids).

Secondary antibody	Host	Brand	Dilutions for mouse retina	Dilutions for HUVECs	Dilutions for WB
Alexa Fluor 488 Phalloidin	-	Life Technologies™ (A12379)	-	1:200*	-
Alexa Fluor 647 Phalloidin	-	Life Technologies™ (A22287)	-	1:50	-
Anti-Mouse HRP Conjugate	Goat	Life Technologies™ (A24524)	-	-	1:5000
Anti-Goat HRP Conjugate	Donkey	Life Technologies™ (A15999)	-	-	1:5000
Anti-Rabbit HRP Conjugate	Goat	Life Technologies™ (G-21234)	-	-	1:5000
Alexa Fluor 647 Anti-Goat	Donkey	Life Technologies™ (A21447)	1:400	-	-
Alexa Fluor 647 Anti-Rabbit	Donkey	Life Technologies™ (A31573)	-	1:400*	-
Alexa Fluor 488 Anti-Rabbit	Donkey	Life Technologies™ (A21206)	-	1:400	-
Alexa Fluor 555 Anti-Rabbit	Donkey	Life Technologies™ (A31572)	1:400	-	-
Alexa Fluor 568 Anti-Mouse	Goat	Life Technologies™ (A21124)	-	1:400	-

12. Spheroids sprouting assay

12.1. Methyl cellulose stock solution

To prepare the methyl cellulose stock (methocell), we used the Methyl cellulose, viscosity 15cp [BioReagent, suitable for cell culture (M7027, Sigma-Aldrich™)]. Methocell must be prepared with caution in order to avoid methyl cellulose debris and, consequently, its low concentration. 1.2g of pure powder was autoclaved in a 500-ml flask containing a clean magnetic stirrer. After, the powder was dissolved in 50mL DMEM 1x medium (61965-026, gibco® by Life Tecnologies, compound with 10% FBS and 1.48% Sodium pyruvate 100mM (11360-039, gibco® by Life Tecnologies)) at 60 °C for 20 min (using the magnetic stirrer). Then, 50 ml DMEM 1x medium (RT) was added to a final volume of 100mL. The solution was mixed and aliquoted and methocell was cleared by centrifugation (5,000xg, 2 h, RT) and the supernatant used for the spheroid culture.

12.2. Sprouting angiogenesis *in vitro*

In order to evaluate cell migration and invasion, the collagen matrix-embedded HUVEC spheroid model (3D model) was implemented in the lab, based in the work of Augustin (Augustin, 2004). At day 0, siRNA transfected confluent monolayers of HUVECs were trypsinized and counted for 150 000

cell/mL. These cells were ressuspended in the corresponding complete culture medium containing 20% methyl cellulose stock solution (see II.12.1), in order to generate size-defined EC spheroids. Spheroids were obtained by spontaneous cell aggregation in hanging drops (20 µL), incubated ON at 37˚C and 5% CO_2. At day 1, spheroids were collected with DMEM 1x and centrifuged at 500xg during 3min. Then, the pellet of aggregates was ressuspended in collagen I, Rat Tail 3mg/mL (A10483-01, gibco® by Life Tecnologies) mixed with some components: NaOH 0.1M; MEM 10x, no glutamine (11430-030, gibco® by Life Tecnologies); HEPES buffer solution 1M (15630-056, gibco® by Life Tecnologies); Sodium Bicarbonate solution 7.5% (25080-060, gibco® by Life Tecnologies); and SFM (described in Table II.8), to obtain a 2mg/mL of final concentration of collagen I. These components ensure the neutralization and the right consistence of this solution, creating an optimal environment for EC spheroids. This solution was equilibrated with 1M NaOH until pH7.4. The ressupended spheroids were placed in a 24 well-plate, where the wells around were filled with H_2O to avoid dehydration. For collagen solution solidification we incubated the plate at 37˚C and 5% CO_2 during 1h. Afterwards 600uL of complete culture medium was added. 24-48h after spheroids were fixed with 4% PFA solution diluted in PBS during 30min with gentle agitation.

Table II.8 - Collagen I solution for sprouting angiogenesis assay. Representative table of components and volumes used in collagen I solution preparation. The represented volumes in table are related with each well (24 well-plate) and condition.

Components	Volume per condition
NaOH 0.1M	41.7µL
MEM 10x	41.7µL
HEPES	8.3µL
Sodium Bicarbonate 7.5%	6.5µL
SFM	68.5µL
Collagen I (3mg/mL)	333.3µL
Total volume 500µL/per well	

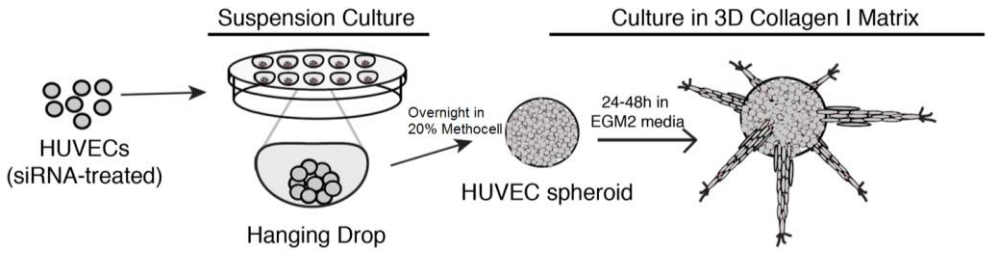

Figure II.2 - Scheme of generation of spheroids. Hanging droplets of transfected HUVECs were performed and then cultured for 24-48h in 3D collagen I Matrix. Figure based from Jakobsson *et al.* (2010).

12.3. Immunofluorescence staining of Spheroids

In order to immunostaining the spheroids, they were removed from the collagen I matrix using the bistoury and spatula and placed in a culture glass dish with PBS. Then, in a binocular dissecting microscope (Carl Zeiss), using forceps and scissors the excess of collagen matrix around the spheroid was carefully removed. Finally, the immunofluorescence staining was performed as in whole-mount retinas (see details in section II.10.1), but with double volumes.

13. Statistical analysis

The statistical analysis was done by one-way Analysis of Variance (ANOVA) using GraphPad Prism 6. We considered values below $p<0.05$ as statistically significant (*, $p<0.05$; **, $p<0.01$; ***, $p<0.001$, ****, $p<0.0001$).

III. RESULTS

1. Selection of candidate genes downstream of the MRTF/SRF pathway

1.1. Transcriptomic analysis of endothelial-specific MRTF/SRF-dependent genes

The MRTF-SRF pathway has been characterized as having an important role during sprouting angiogenesis. Claudio Franco's lab performed previously an unbiased Affymetrix microarray-based characterization of the MRTF/SRF-transcriptome in HUVECs. The aim was to discover which genes downstream of SRF are important for tip cell function. This approach was performed using specific siRNAs to knockdown separately SRF and MRTFs in HUVECs. Moreover, cells in each condition were either unstimulated or stimulated for 30min with 50ng/mL of VEGF-A. The Venn diagram (Figure III.1) highlights the genes downregulated when compared to control samples for each specific category. This approach identified a core of genes (113) significantly downregulated in the four different conditions. Gene Ontology analysis demonstrated that the selected genes are closely linked to actin cytoskeleton processes (Figure III.2).

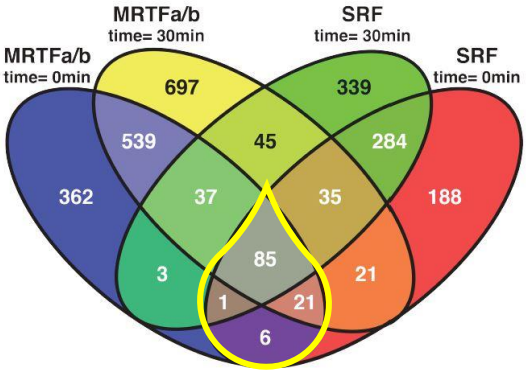

Figure III.1 - Venn Diagram for downstream of the MRTF/SRF signaling. Downregulated genes in different conditions when compared to the transcriptome profile of HUVEC treated with siRNA against SRF or MRTFs and control siRNA under equivalent treatments. Selected genes correspond to genes downregulated in 4 conditions.

Process name	p.val	ratio
Cytoskeleton_Actin filaments	1.34E-09	'26/176
Cytoskeleton_Regulation of cytoskeleton rearrangement	1.26E-05	'20/181
Cell adhesion_Integrin-mediated cell-matrix adhesion	3.14E-04	'19/210
Development_EMT_Regulation of epithelial-to-mesenchymal transition	4.23E-04	'19/215
Cell adhesion_Attractive and repulsive receptors	1.73E-03	'15/170

Figure III.2 - Gene Ontology analysis for the 113 selected genes. The most representative processes in which selected genes are involved relate to regulation of actin cytoskeleton dynamics and cell migration processes.

In this context, the first goal of my project was to identify specific genes of interest downstream of SRF from the 113 core of candidate genes previously identified. In order to restrict our candidate gene pool, we selected the most important genes following the specific criteria (at least 3 out of 4):

(1) The germline knockout (KO) of the gene of interest should be lethal or not reported; and endothelial-specific KO was not yet reported.

(2) Genes should have been previously linked to cell migration or actin cytoskeleton regulation;

(3) The promoter region of the gene of interest should contain SRF-binding sites identified in the ENCODE project (ENCyclopedia Of DNA Elements);

(4) The RNA or protein of the gene of interest should be expressed in endothelial cells and previously described at the Euroexpress (a transcriptome atlas database for the mouse embryo) and Protein Atlas Database.

As a result, we selected a subset of 13 downstream target genes (described in Table III.1).

Table III.1 - Selected candidate genes. Representative table of candidate genes selected in this study and their main functions.

Name/Gene ID (from NCBI)	Official Full Name (from NCBI)	Main functions of encoded protein
ACTR3 (Gene ID: 10096)	ARP3 actin-related protein 3 homolog (yeast)	Specific function has not yet been determined. However, the protein is known to be a major constituent of the ARP2/3 complex (from NCBI).
FLNA (Gene ID: 2316)	filamin A, alpha	Actin-binding protein involved in cytoskeleton remodeling affecting cell shape and migration (from NCBI).
LIMA1 (Gene ID: 51474)	LIM domain and actin binding 1	Cytoskeleton-associated protein that inhibits actin filament depolymerization and cross-links filaments in bundles (from NCBI).
MICAL2 (Gene ID: 9645)	microtubule associated monooxygenase, calponin and LIM domain containing 2	Nuclear monooxygenase that promotes depolymerization of F-actin regulating of the SRF signalling pathway (SRF:MKL1/MRTF-A-dependent gene transcription) (from UniProtKB/Swiss-Prot)
MYH9 (Gene ID: 4627)	myosin, heavy chain 9, non-muscle	Conventional non-muscle myosin involved in cytokinesis, cell motility and maintenance of cell shape (from NCBI).
MYL9 (Gene ID: 10398)	myosin, light chain 9, regulatory	Myosin light chain regulates muscle contraction by modulating the ATPase activity of myosin heavy chain heads (from NCBI).
TAGLN2 (Gene ID: 8407)	transgelin 2	The specific function has not yet been determined, although it is thought to be a tumor suppressor (from NCBI).
TPM1 (Gene ID: 7168)	tropomyosin 1 (alpha)	Binds to actin filaments in muscle and non-muscle cells. In non-muscle cells is implicated in stabilizing cytoskeleton actin filaments (from UniProtKB/Swiss-Prot).
TPM2 (Gene ID: 7169)	tropomyosin 2 (beta)	This gene encodes beta-tropomyosin, a member of the actin filament binding protein family and have the same main functions of TPM1 (From NCBI)
TPM4 (Gene ID: 7171)	tropomyosin 4	This protein have the same main functions of TPM1 (From NCBI)
FILIP1 (Gene ID: 27145)	filamin A interacting protein 1	This protein acts through a filamin-A/F-actin axis. Controls the start of neocortical cell migration. (from UniProtKB/Swiss-Prot).
NEXN (Gene ID: 91624)	nexilin (F actin binding protein)	Filamentous actin-binding protein that is involved in cell adhesion and migration (from NCBI).
PALLD (Gene ID: 23022)	palladin, cytoskeletal associated protein	Cytoskeletal protein that is required for cytoskeleton organization and it is involved in the control of cell shape, adhesion, and contraction (from NCBI).

1.2. Validation of MRTF/SRF-dependent candidate genes

To confirm if the selected genes were indeed downstream of the SRF pathway, we extracted RNA and protein from HUVECs knocked down for SRF or MRTF-A/B (MRTFs) and analyzed the expression of the selected candidates by qPCR (Figure III.3) and by WB (Figure III.4). The combined knockdown of both MRTF-A and MRTF-B in HUVECs led to decreased expression of *ACTR3*, *FLNA*, *LIMA1*, *MICAL2*, *MYH9*, *MYL9*, *TAGLN2*, *TPM1*, *TPM2*, and *TPM4* (Figure III.3). Similar to the results observed in SRF knockdown experiments. However, no significant change in *FILIP1*, *NEXN* and *PALLD* was observed in both settings. This analysis allowed us to exclude these 3 genes and confirmed the specific downregulation of the other 10 candidates (Figures III.3 and III.4). So, from this initial analysis we were able to select a core of 10 genes that filled all the chosen criteria. We were not able to perform WB analysis for some of the genes because the purchased antibodies did not give consistent results.

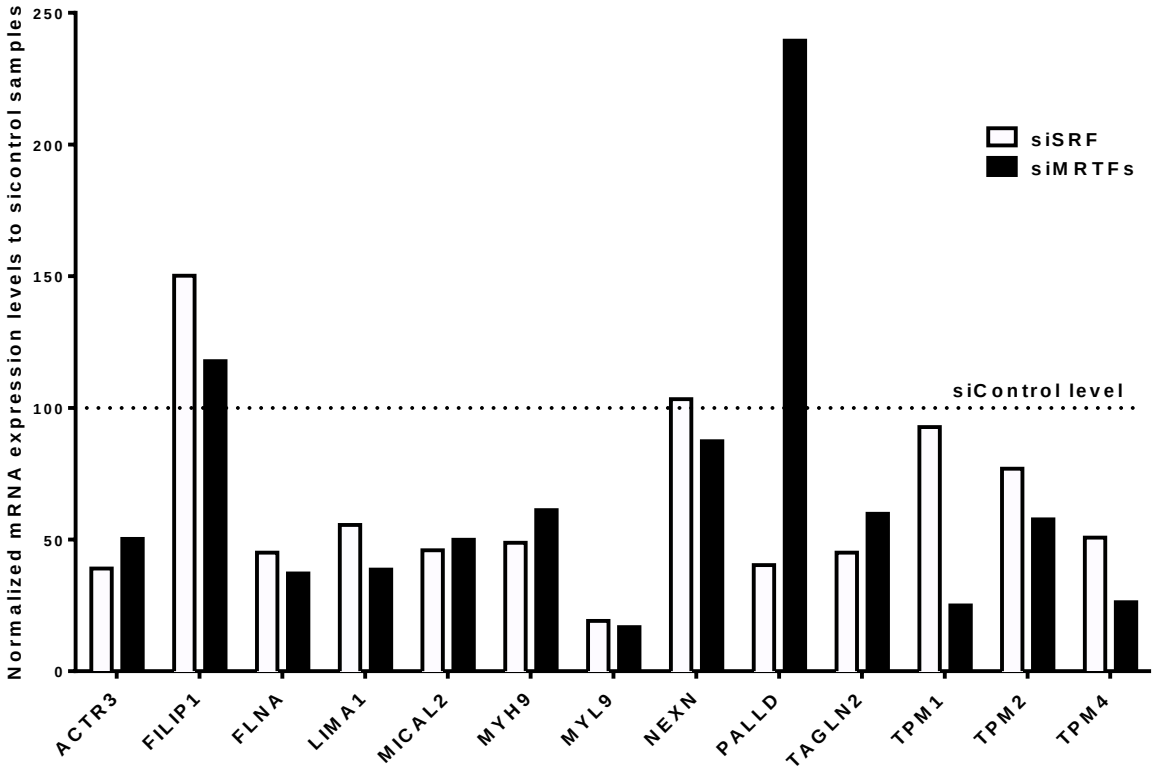

Figure III.3 - qPCR analysis of selected candidate genes. Analysis of the expression levels of the selected genes confirming a significant downregulation of 10 out of 13 genes (FILIP1, NEXN and PALLD did not showed a significant downregulation). Line points show the control levels of siControl samples. GAPDH was used as housekeeping gene for control.

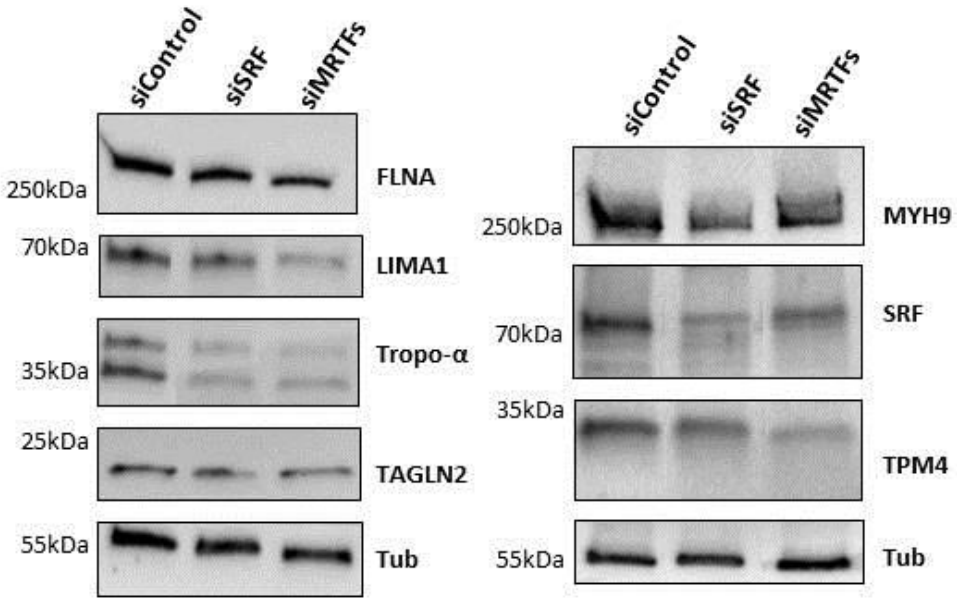

Figure III.4 - Western Blot analysis of some the selected candidate genes. Analysis of the protein expression levels of some candidates [FLNA, LIMA1, Tropomyosin-α (Tropo-α, also known TPM1), TAGLN2, MYH9 and TPM4] confirming a downregulation. Tubulin (Tub) was used as loading control in WB.

2. Functional validation of positive candidate genes

2.1. Setting-up a siRNA-based functional screen

SRF regulates the expression of several proteins, including actin regulatory proteins involved in EC migration and invasion (Franco et al., 2013), thus we were expecting that some of the selected candidate genes would affect endothelial cell behavior. In order to validate the functionality of candidate genes in *in vitro* cell migration assays, we purchased 3 specific siRNAs for each selected SRF-target gene. *MYL9* was previously demonstrated that is a MRTF/SRF-dependent target gene and that it was involved in endothelial cell migration. However, it did not phenocopy SRF-dependent tip cell filopodia deficiency (Franco *et al.*, 2013). Thus, we decided to focus our attention in the study of the 9 remaining candidate genes.

We then confirmed the efficiency of each single siRNA by qPCR together with cell viability tests. According to these two analyses and for each candidate gene, one effective siRNA was carefully selected (siMYH9-3, siFLNA-3, siTPM1-2, siTPM2-2, siTPM4-1, siTAGLN2-3, siLIMA1-2, siACTR3-1, siMICAL2-1) taking into account the knockdown efficiency (Figure III.5) and also the cell viability after HUVEC transfection (evaluation of dead cells *vs.* viable cells) (Table III.2).

Table III.2 - Viability tests in cultured HUVECs. Representative table of HUVECs mortality, after transfection (24-48h), with different siRNA [3 for each candidate gene (siRNA-1, -2 and -3)]. The symbol (-) represents few cell death events; other degrees of cell death are represented, from + to ++++ (a lot of cell death events).

siRNAs for candidate genes	siMYH9-1	siMYH9-2	siMYH9-3	siFLNA-1	siFLNA-2	siFLNA-3	siTPM1-1	siTPM1-2	siTPM1-3	siTPM2-1	siTPM2-2	siTPM2-3	siTPM4-1	siTPM4-2	siTPM4-3	siTAGLN2-1	siTAGLN2-2	siTAGLN2-3	siLIMA1-1	siLIMA1-2	siLIMA1-3	siACTR3-1	siACTR3-2	siACTR3-3	siMICAL2-1	siMICAL2-2	siMICAL2-3
Mortality	+	+	+	-	+	+	-	+	-	-	-	+++	++++	-	+	-	-	-	+	++	+++	-	+	+	+	++	+

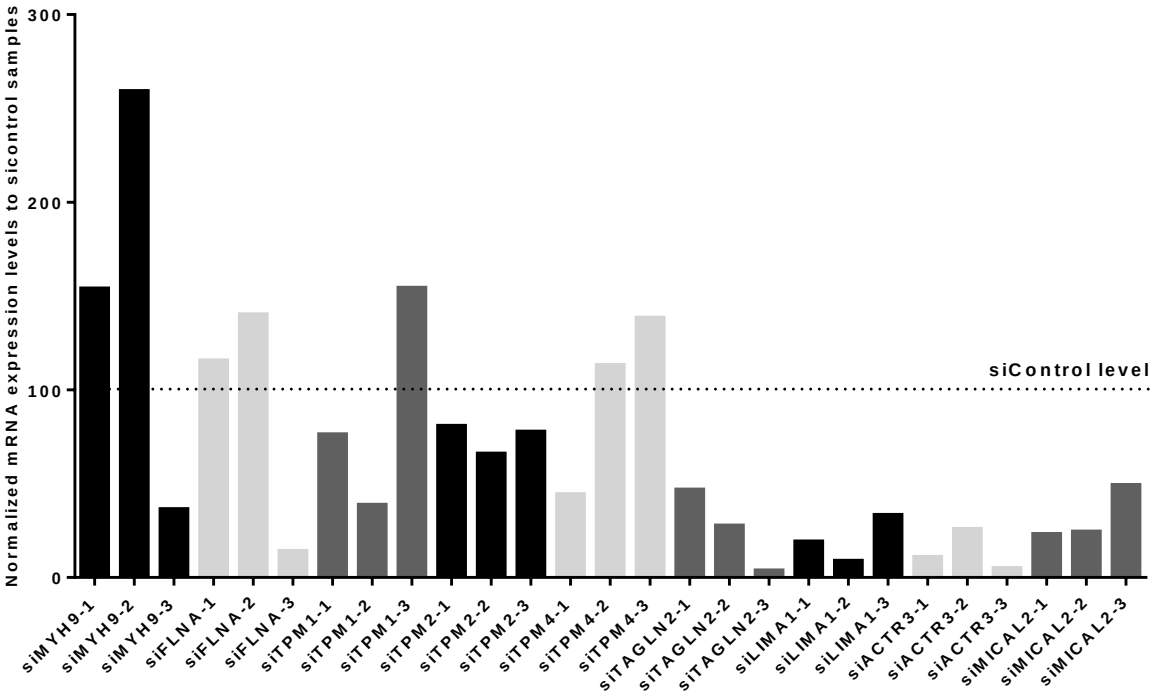

Figure III.5 - Analyze of the efficiency of each siRNA by qPCR. Analysis of the expression levels of selected genes after transfection with each siRNA for each candidate gene. We managed to confirm the downregulation for all genes with at least one siRNA. Line points show the control levels of siControl samples. GAPDH was used as housekeeping gene for control.

Our analysis led to the exclusion of *LIMA1* and *TPM4* because of the low cell viability after siRNA transfection in each of the 3 different siRNAs. *MICAL2* was also excluded because of a recent study from Lundquist and collegues showing that MICAL2 regulates SRF/MRTF-A-dependent gene transcription, with a redox modification of nuclear actin (Lundquist *et al.*, 2014), thus affecting SRF/MRTF output rather than regulating actin dynamics directly. Therefore, we selected 6 genes (*ACTR3*, *FLNA*, *MYH9*, *TAGLN2*, *TPM1*, *and TPM2*) for further analysis using different *in vitro* assays.

2.2. Scratch-wound cell migration assay

To evaluate the impact of each gene in cell migration, we used the in vitro scratch-wound assay. In this assay, a wound is made in a confluent HUVEC monolayer and the closure is measured over time. Scratch-wound assay allowed us to measure cell migration speed, invasion capacity and actin cytoskeleton structure content.

First, we performed the scratch-wound assay and capture images at the beginning and at the end of cell migration (16h), just before the endothelial cells closed the wound. By quantification the total migration length in bulk endothelial cell surfaces, we determined a rough measure for endothelial cell migration. These results are shown in Figure III.6, where we observed that when knocked down, several genes significantly affect the capacity of endothelial cells to close the wound (decrease of migration capacity). MYH9, ACTR3 and TAGLN2 knockdowns caused a significant strong reduction in overall closure of wound. The impairment in cell migration was similar in magnitude to the observed effect of SRF or MRTF-A/B knockdown (Figure III.6). TPM1 knockdown also affected endothelial cell migration, but with less intensity than the previously mentioned genes. TPM2 and FLNA knockdowns did not significantly affect endothelial migration (Figure III.6).

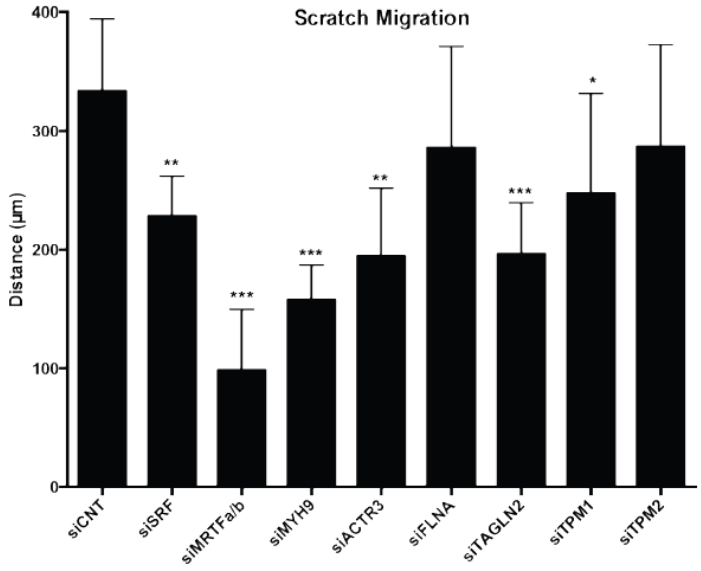

Figure III.6 - Analysis of cell migration in the scratch-wound assay. The scratch was performed after overnight starvation. Closured of the wound was measured 16 hours after. *, p<0.05; **, p<0.01; ***, p<0.001.

In order to get further insights on the migratory behavior of HUVECs, we performed live-imaging during 16h (every 10min) and quantified total distance, average and maximum speeds and straightness of the migratory path (Figure III.7 and data not shown). Together, these results showed that MYH9 and ACTR3 knockdowns lead to decrease of endothelial cell migration and speed (with a significant *p-value* <0.01 or *p-value* <0.001). Therefore, *MYH9* and *ACTR3* appear to be the most likely genes downstream of SRF signaling that regulates endothelial cell migration.

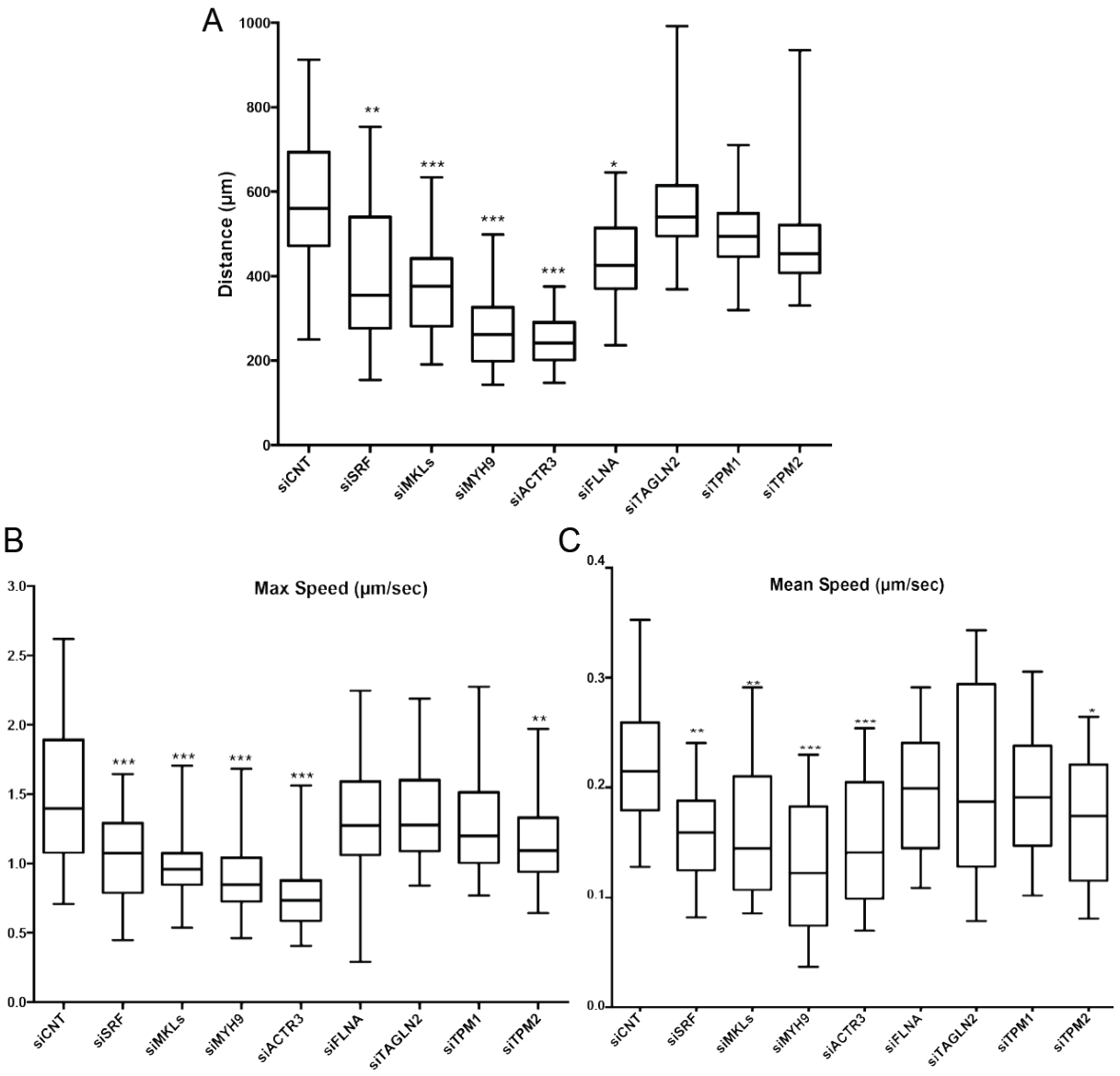

Figure III.7 - Analysis of cell migration in the scratch wound assay. The scratch was performed after overnight starvation. Closured of the wound was measured 16 hours after with time point to each 10min. *, p<0.05; **, p<0.01; ***, p<0.001.

2.3. Cell Cytoskeleton architecture

MRTF/SRF pathway is a main regulator of the cellular actin cytoskeleton. We therefore next analyzed the cytoarchitecture of endothelial cells when depleted for each of 6 specific candidate genes and compared to control and SRF or MRTFs-depleted HUVECs. We quantified the levels of actin filaments, focal adhesions and cellular junctions. To do so, we labeled HUVECs *in vitro* with antibodies against vinculin - a focal adhesion molecule; zona occludens protein 1 (ZO1) - a tight junctional molecule; together with phalloidin – a probe that binds to filamentous actin (F-actin). We quantified the total intensity for each staining and analyzed some morphological parameters, such as the morphology of actin filaments, the shape of cells and the filamentous actin content in HUVECs treated with different siRNAs (Figure III.8 and Figure III.9). In *MYH9* depleted cells we observed a decrease in immunofluorescence intensities of vinculin and phalloidin ($p<0.01$ and $p<0.001$, respectively), which means that MYH9 is not only regulating the F-actin content, but also the focal adhesions (Figure III.9). We also observed a similar decrease in the content of actin filaments and in the intensity of vinculin staining in ACTR3 depleted cells ($p<0.001$) (Figure III.8 and Figure III.9). Decreased expression of the remaining genes didn't affect significantly the levels of F-actin content and organization, and vinculin intensity.

In the case of MYH9-depleted cells, we could see that cells presented a rounded shape and an altered organization of actin filaments, *i.e.*, absence of transversal actin cables (Figure III.8). siACTR3 treated cells showed a more spindle shape, looking more siControl than MRTF or SRF-depleted cells. The other genes didn't significant affected cell shape when compared to siControl-transfected cells. Thus, phenotypically, MYH9 depleted cells resemble SRF or MRTFs knocked down cells, morphologically and structurally. Therefore, we decided to focus our attention in *MYH9* as the main candidate gene, since its absence resulted in a phenotype more closely related to SRF deficient HUVECs.

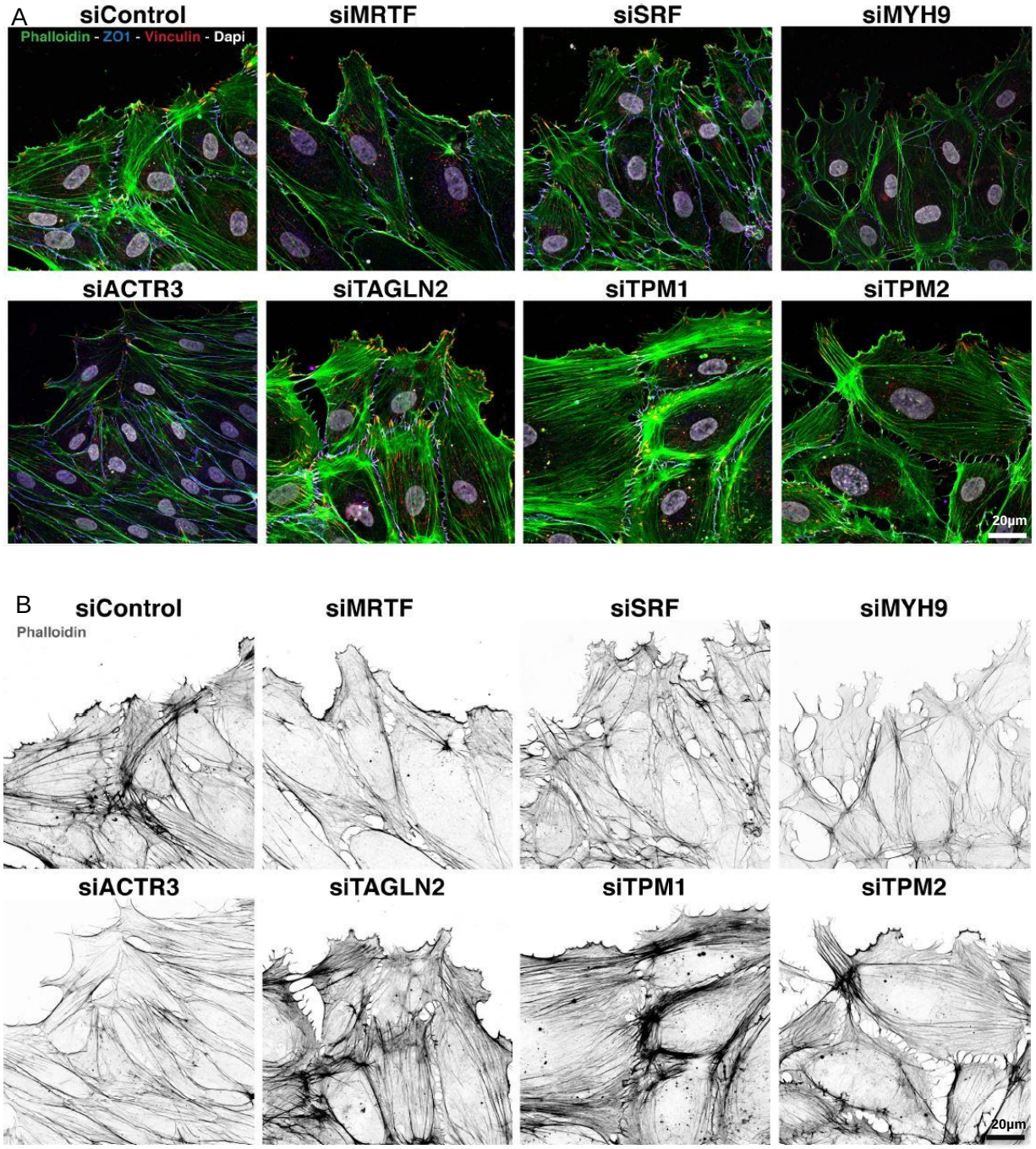

Figure III.8 - Analysis of cell migration in the scratch wound assay. **A-B**, Cells were stained for phalloidin (A, green; B, grey), vinculin (red), ZO1 (blue) and DAPI (upper panel). siMYH9 siACTR3 conditions exhibit defects in actin polymerization rate.

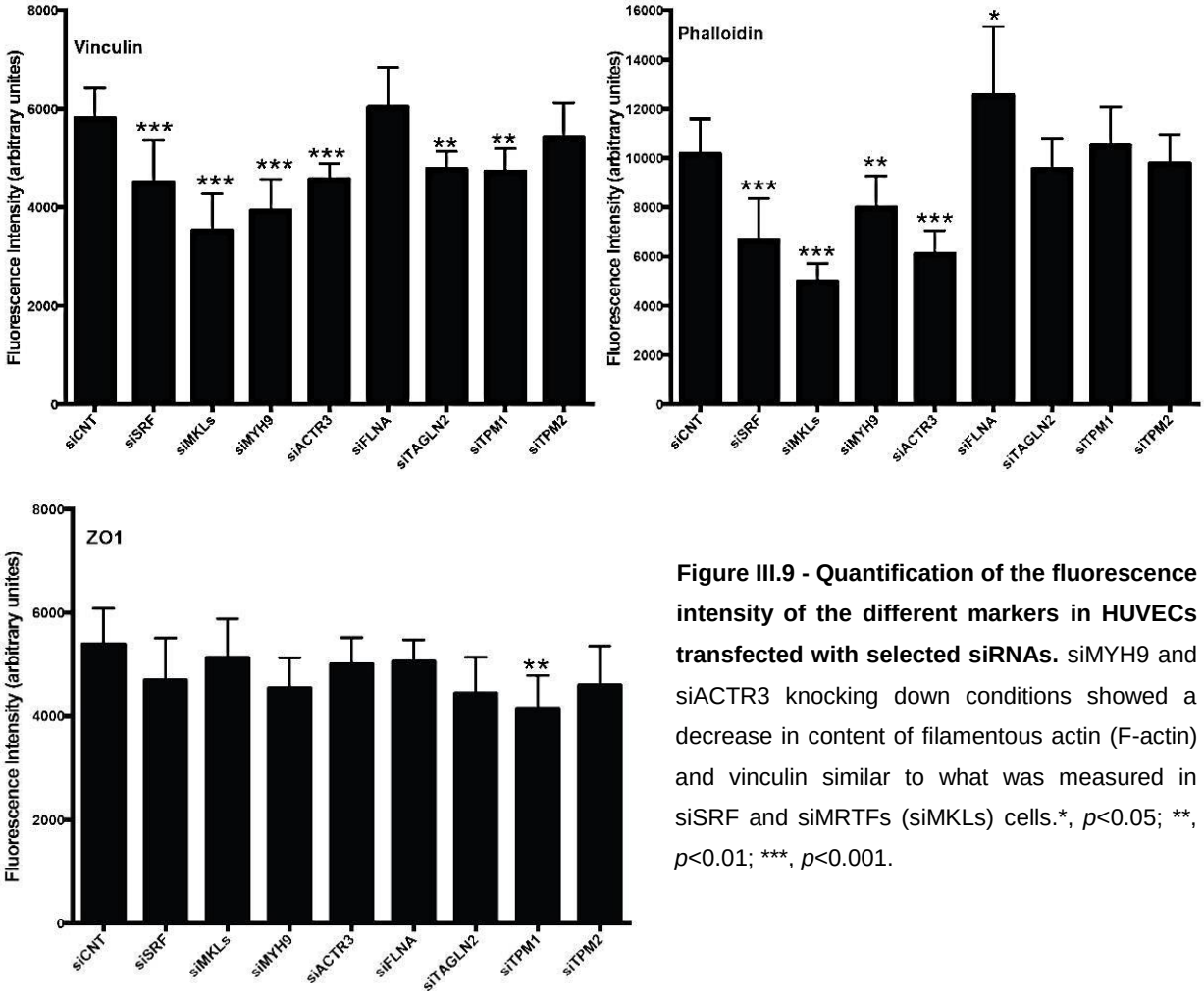

Figure III.9 - Quantification of the fluorescence intensity of the different markers in HUVECs transfected with selected siRNAs. siMYH9 and siACTR3 knocking down conditions showed a decrease in content of filamentous actin (F-actin) and vinculin similar to what was measured in siSRF and siMRTFs (siMKLs) cells.*, $p<0.05$; **, $p<0.01$; ***, $p<0.001$.

3. MYH9 is a major actin regulator downstream of the MRTF/SRF pathway

3.1. MYH9 function is essential for efficient endothelial sprouting

In order to confirm the efficiency of *MYH9* knockdown, we performed additional immunofluorescence staining and western blots. We observed a pronounced decrease in MYH9 staining in cells treated with siMYH9 comparable to the reduction detected in SRF deficient cells (Figure III.10). We also observed through WB analysis a significant decrease in MYH9 protein levels ($p<0.001$) in MYH9, SRF and MRTFs depleted HUVECs (Figure III.11 and III.4). Moreover, SRF and MYH9 deficient HUVECs have a decrease in protein levels of pMLC and MLC2 (regulatory light chain of myosin), confirming a defective status of the Myosin complex in endothelial cells (Figure III.11).

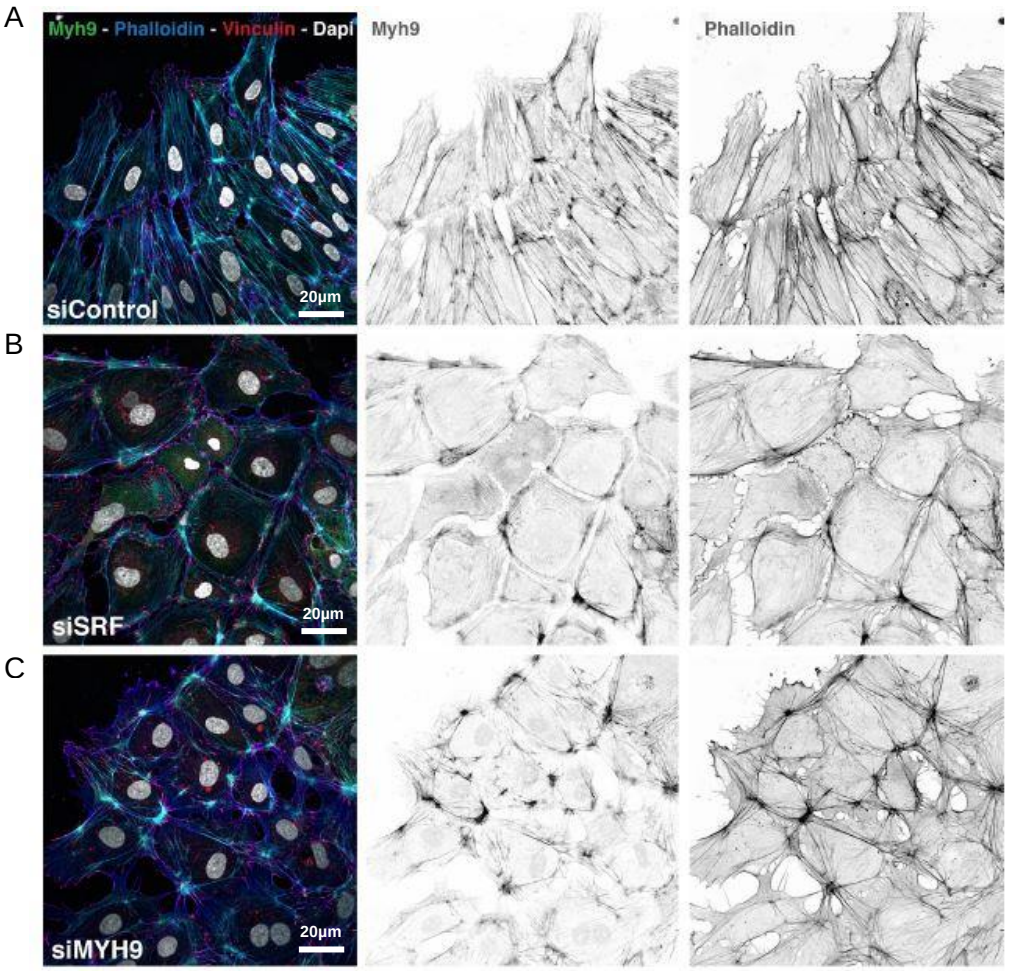

Figure III.10 - MYH9 staining in HUVECs transfected with selected siRNAs (siSRF and siMYH9). **A**, HUVECs in a control situation, showed a staining for Phalloidin, vinculin and MYH9. **B**, MYH9 deficient cells showed a decrease in content of F-actin and MYH9. **C**, Similar reduction was noticed in siSRF HUVECs.

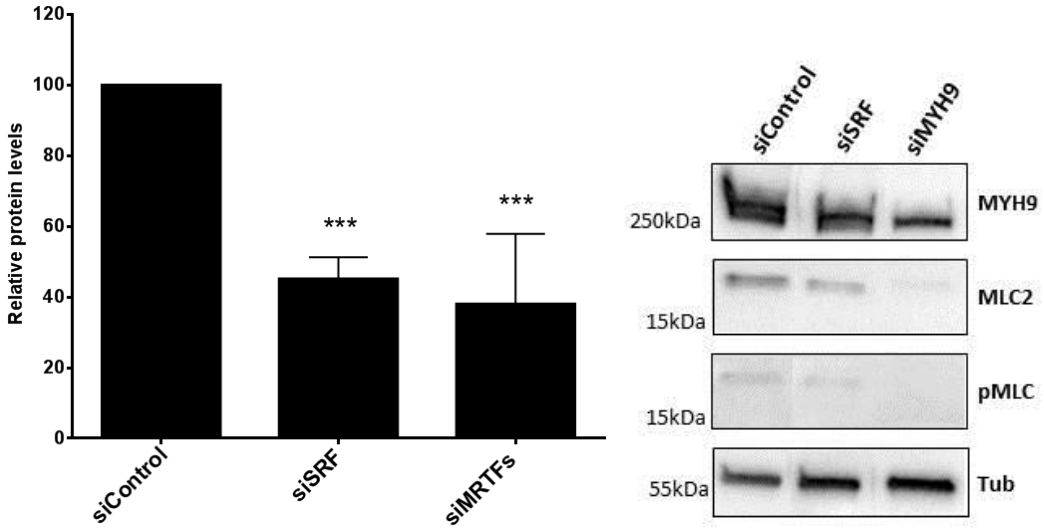

Figure III.11 – Relative protein levels in HUVECs transfected with different siRNAs. Left panel, quantification by WB showed a decrease of MYH9 level in siSRF and siMRTFs HUVECs. ***, $p<0.001$. Right panel, WB analysis showed decrease of MYH9, MLC2 (MYL9) and pMLC levels.

Next, we evaluated the function of MYH9 in endothelial 3D sprouting assays. For this, we implemented the HUVEC-spheroid 3D sprouting assay. With this method we confirmed that spheroids derived from HUVECs depleted of SRF or MYH9 had similar defects in vascular sprouts elongation (p<0.0001) (Figure III.12). Interestingly, we observed that MYH9 is highly enriched in endothelial tip cell, with particular high intensity at the leading edge. The levels of MYH9 correlated with increased intensity of phalloidin-staining, which indicates a higher content in filamentous actin. (Figure III. 12 in upper panel). Therefore, we concluded that MYH9 is essential for endothelial sprouting and invasion in both 2D and 3D environments.

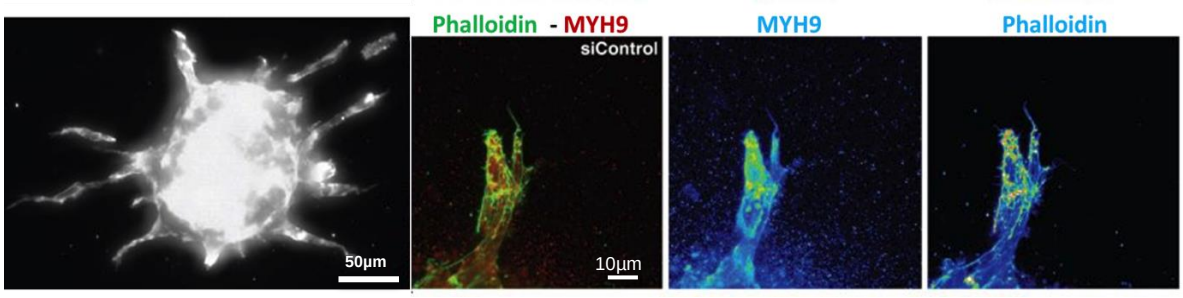

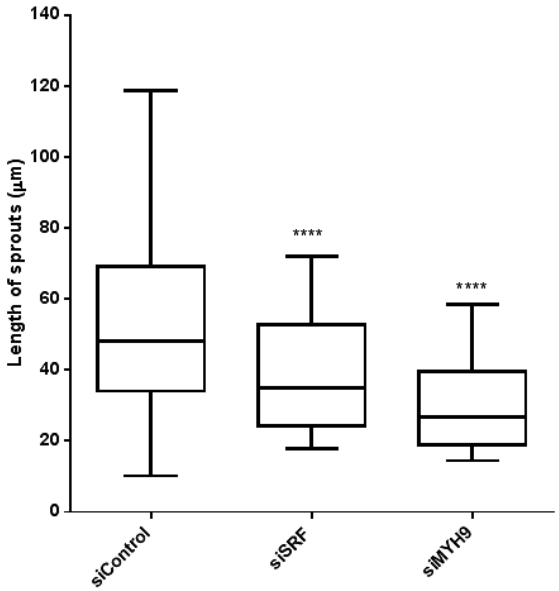

Figure III.12 - HUVEC spheroid sprouting analysis. Upper panel: Representative images of an endothelial tip cell arising from a spheroid, stained for actin and MYH9. Similarly to the *in vivo* situation, with this approached was observed that MYH9 is highly active in the tip cell, with particular high intensity at the leading edge (best visualized in the pseudocolor panels. **Left panel**, quantification of length of vascular sprouts shows that siMYH9 and siSRF transfected HUVECs have similar defects in the elongation of sprouts. ****, p<0.0001.

3.2. Re-expression of MYH9 rescues SRF-deficient phenotype

To further validate that MYH9 plays an essential function downstream of SRF signaling, we sought to rescue the phenotype in SRF-depleted HUVECs by forced expression of MYH9. We overexpressed a full-length version of MYH9 tagged with GFP in the N-terminal (MYH9-GFP) in SRF depleted HUVECs to assess whether MYH9 could be sufficient to rescue the effects induced by the absence of SRF. Through immunofluorescence analysis we demonstrate that MYH9 rescued partially the actin polymerization defects induced by the absence of SRF (p<0.05). Thus, this result reinforces the idea that MYH9 plays a central role in SRF-dependent transcriptome (Figure III.13).

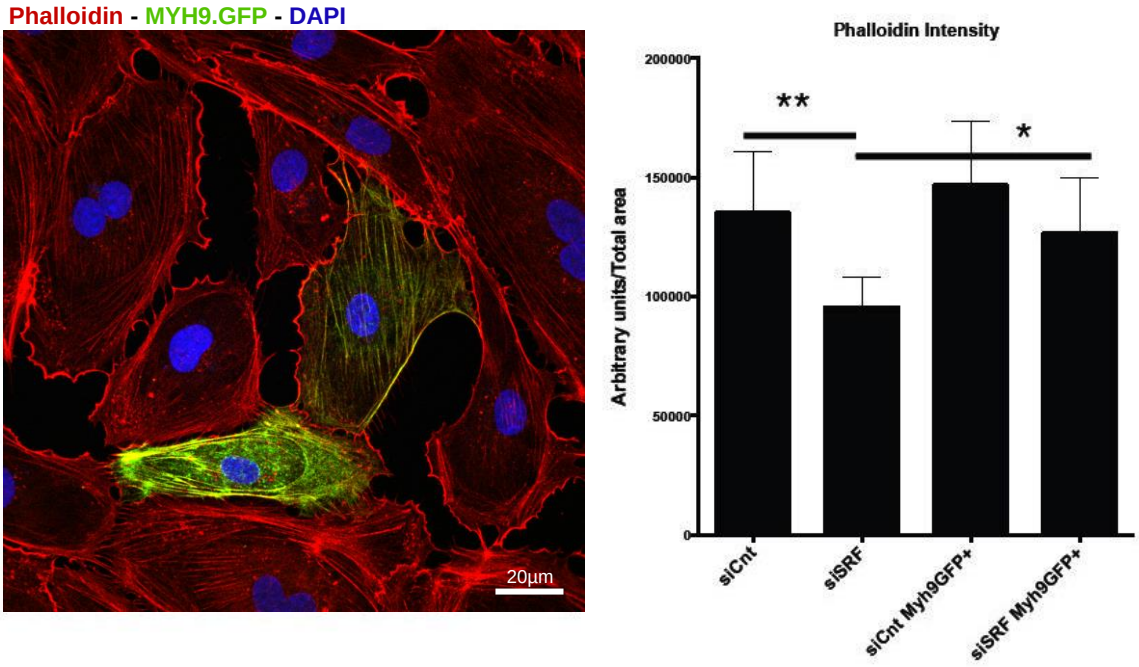

Figure III.13 - Overexpression of MYH9-GFP compensates SRF-deficiency. HUVECs overexpressing MYH9-GFP (green cells) and then labelled for phalloidin (red cells) and dapi (nuclei), left panel. Right panel shows the quantification of the level of phalloidin staining in cells targeted for siControl, siSRF with or without transfection with p-CAG-GFP-MYH9 plasmid. *, p<0.05; **, p<0.01.

3.3. MYH9 is enriched in endothelial tip cells *in vivo*.

Finally, we analyzed by immunofluorescence the location of MYH9 in the retinal vasculature of LifeAct-GFP mouse lines. It is important to note that the LifeAct-GFP transgene is highly expressed in retinal ECs, allowing visualization of the actin cytoskeleton specifically in the vasculature (Fraccaroli *et al.*, 2012). Interestingly in this analysis, we observed that MYH9 is highly expressed by endothelial tip cells and that its expression is specifically located at the base of endothelial filopodia in these cells (Figure III.14). These results suggest a novel feature for MYH9.

Thus, all data suggest that MYH9 has an important role in SRF signaling, in cell migration, invasion, cytoskeleton dynamics and has probably an important link to tip cell filopodia.

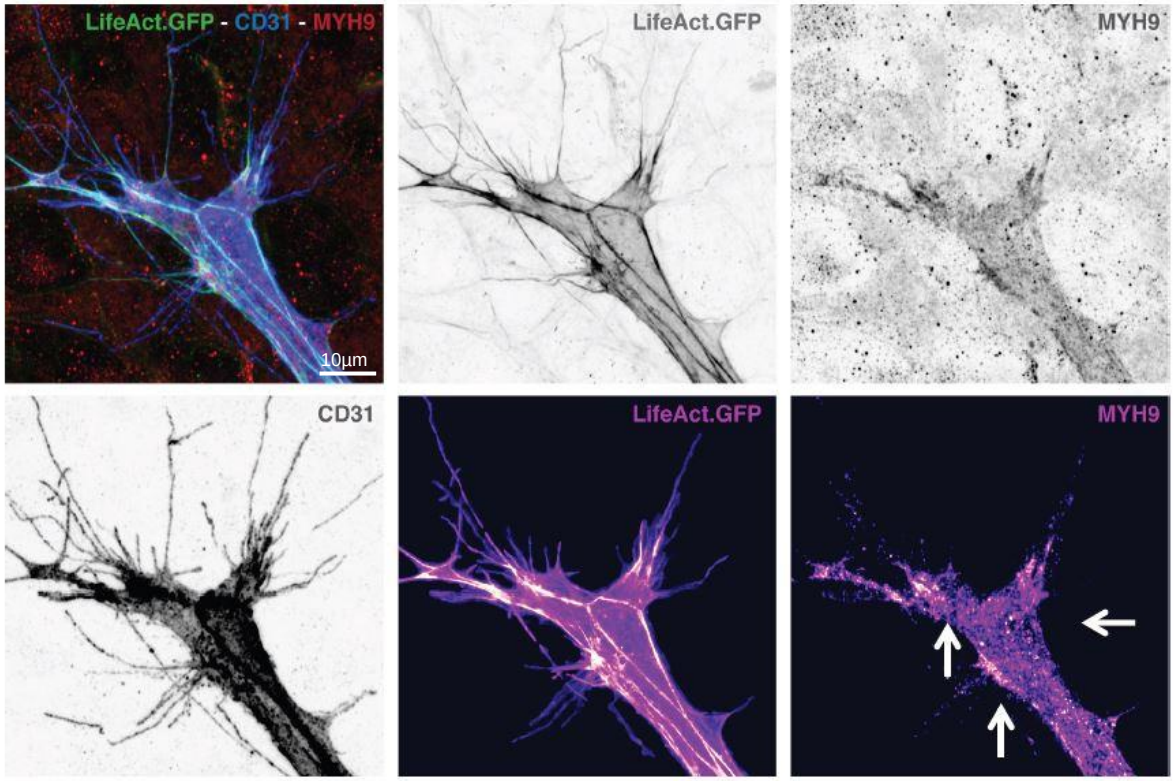

Figure III.14 - Retinal endothelial cells analysis. Representative image of an endothelial tip cell from a LifeAct-GFP mouse line stained for the endothelial cell marker CD31 (blue or grey), labeling the endothelial cells and MYH9 (red, grey or pseudocolored). Actin filaments can be visualized in green or grey. Strongly intensity was observed in MYH9 label at the base of endothelial filopodia (arrows).

IV. DISCUSSION

During angiogenesis, endothelial cells need to become motile in order to invade avascular tissues. These processes require the presence of SRF in endothelial cells, a transcription factor highly expressed in endothelial cells at the sprouting front, that has been previously showed to be involved in tip cell invasion towards VEGF-A gradient (Franco *et al.*, 2013). SRF has been suggested as a regulator of many features of actin cytoskeleton biology related to cell migration, together with MRTFs cofactors (Franco *et al.*, 2013; Miano *et al.*, 2007). In this sense, it is important to understand which cytoskeletal proteins are involved in the regulation of endothelial tip cell invasion, downstream of SRF signaling. As such, in the present work, we used siRNA technology in order to identify and characterize the function of specific SRF-downstream genes involved in endothelial cell migration and invasion. Our approach was focused on the evaluation of candidate genes shortlisted from a pool of candidates previously obtained by an unbiased microarray analysis.

Our results showed that knockdown of *MYH9* and *ACTR3* lead to a decrease in cell migration similar to the one observed in SRF and MRTFs depleted HUVECs. Endothelial cell migration is essential to angiogenesis in the context of physiological and pathological angiogenesis (Michaelis, 2014; Lamalice et al., 2007), these results strongly suggest that these two genes might be important for sprouting angiogenesis. *ACTR3* (also known as *ARP3*) encodes actin-related protein 3 that is known to be a component of the ARP2/3 complex (Nürnberg *et al.*, 2011), an actin nucleator that has been implicated in *de novo* actin polymerization and branching of the actin network (Blanchoin *et al.*, 2014; Pollard and Cooper, 2009). *MYH9* (non-muscle myosin heavy chain IIA – NMHCII-A) is one out of three different genes that encode the non-muscle II heavy chain proteins of non-muscle myosin II (Vicente-Manzanares *et al.*, 2009). Myosin motor proteins, such as NMII-A, are also implicated in cell migration and in the control of cell adhesion and contractility (Vicente-Manzanares *et al.*, 2009). Myosins are able to generate force between actin filaments, promoting the contraction of cell structures (Lecuit *et al.*, 2011; Pollard and Cooper, 2009). Physical changes in appearance, shape, position and contact with extracellular structures including other cells, require the proper cellular motile functions. In fact, it has been shown that during cell migration there is a constant remodeling of the actin cytoskeleton in order to form different actin-based structures at the front and rear of the cell (such as filopodia, lamellipodia, or stress fibers). In this sense, motile functions need many dynamic cell behaviors, such as cell migration, guided movement, adhesion and contraction (Olson and Nordheim, 2010). So it makes sense that the knocked down of these two genes not only affected the normal cytoskeleton organization but also influenced the migratory capacity of endothelial cells.

Interestingly, morphological analysis showed that MYH9 depleted cells exhibit a phenotype more similar to SRF depleted HUVECs than ACTR3 depleted cells. In fact, is known that F-actin interacts with non-muscle myosin II (NMII) to induce cell shape change in endothelial cells (Strilić *et al*., 2009). So, it makes sense that MYH9 depleted HUVECs have impaired cell morphology. Confirming the important relevance of MYH9 downstream of MRTF/SRF signaling, we demonstrated that MYH9 is able to partially rescue the actin polymerization defects in SRF depleted cells. Thus, our results

revealed that MYH9, a core protein of the myosin complex, could be essential for cytoskeleton dynamics downstream SRF/MRTF signaling and we decided to focus our attention in this protein in particular. However, we do not exclude the possibility for an important role of ACTR3 in endothelial tip cells *in vivo*, downstream of SRF transcriptional activity.

The analysis of cell migration and invasion by HUVEC-spheroid sprouting assay showed that SRF and MYH9 depleted HUVECs had similar defects in vascular sprout elongation, supporting the idea that MYH9 is an important protein involved in sprouting angiogenesis. Interestingly, with this approach that mimics the *in vivo* situation, we observed that MYH9 is highly active in the tip cell, with particular high intensity at the leading edge. In accordance, a recent report showed that MYH9 assembles at the leading edge, where it promotes contractile actin arcs (Pasapera *et al.*, 2015), therefore supporting the idea that NMII-A is not only essential for cell rear contraction and retraction, but also a key at the leading edge.

Curiously, in our *in vivo* mouse retina model, we observed that MYH9 is highly expressed by endothelial tip cells, specifically at the base of endothelial filopodia in these cells. These results suggest a novel feature for MYH9 in endothelial cells. MYH9 has been seen at the front of the cell in the leading-edge, promoting actin bundling, maturation and turnover of adhesions behind the lamellipodia (Juanes-Garcia *et al.*, 2015; Vicente-Manzanares *et al.*, 2007) that contrast with our results in the rear of filopodia. In this sense we suggest that the localization of MYH9 in the base of filopodia could be necessary for its stabilization in order to tip cells migration and invasion behavior during angiogenesis. However, further experiments must be conducted in order to validate this hypothesis.

Under VEGF stimulation, effective elongation of the sprout appears to be driven by the velocity, orientation and directionality of endothelial cell migration (Iruela-Arispe and Davis, 2009). Endothelial tip cells play a central role in sprouting angiogenesis. During new sprout formation, tip cells have high demands for a robust and active cytoskeleton for appropriate cell invasion and migration.

In this context, our results show that SRF/MRTF signaling regulate tip cell behavior, including cell migration and invasion, through regulation of MYH9 levels. Elevated MYH9 expression levels foster functional cytoskeleton dynamics and stabilization of tip cell filopodia protrusions (Figure IV.1). It is known that VEGF plays a major role in the regulation of key events required for several functions of endothelial cells, as a potent angiogenic agent, such as endothelial cell proliferation and migration (Lamalice *et al.*, 2007). In this context, VEGF induces the activation of VEGFR2 in tip cells, which promotes in its turn the activation of RhoGTPases, including Rac1, Cdc42 and RhoA. This signaling axis promotes polymerization of actin filaments and, consequently, decreases the cytosolic pool of G-actin, leading to the nuclear translocation of MRTFs and transcription of SRF-target genes, such as genes encoding cytoskeletal and contractile proteins (Franco and Li, 2009; Miano et al., 2007). Thus, our work suggests that MYH9 is the main SRF-target that promotes the motile and invasive behavior of endothelial tip cells, regulating cytoskeleton organization and stabilization of tip cell filopodia (Figure IV.1). How these events are related to MYH9 function during sprouting angiogenesis remains yet to be uncovered.

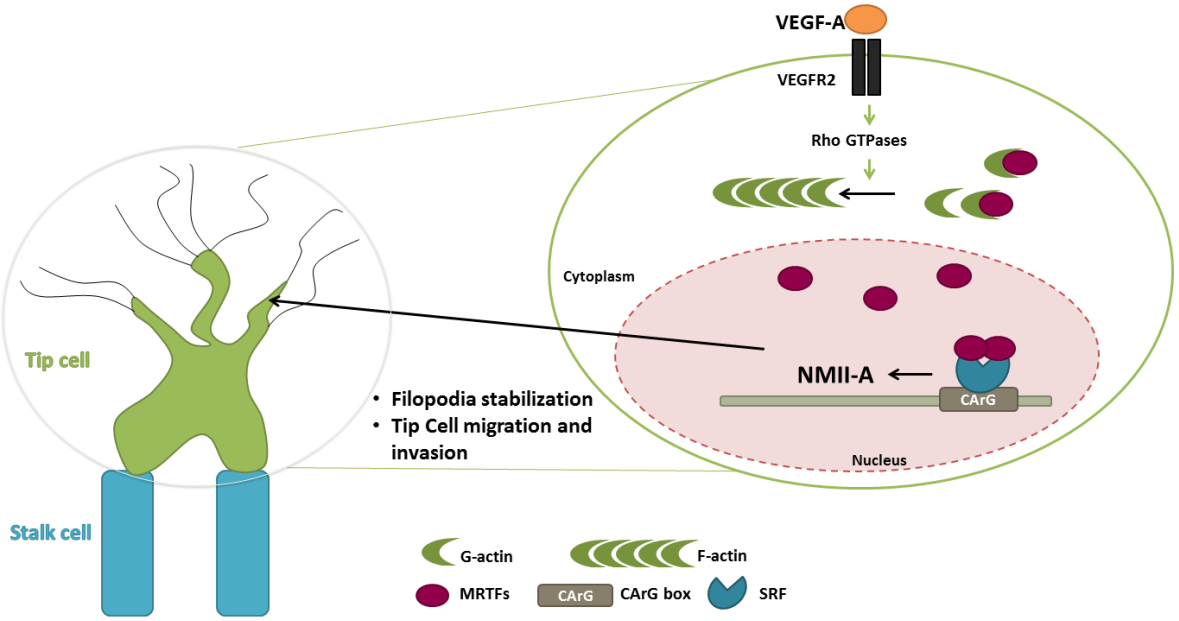

Figure IV.1 - Schematic representation of SRF signaling inducing NMII-A activity. This signaling pathway is initiated by VEGF-A stimulation that can modulate Rho GTPases activity. Rho GTPases activity stimulates the F-actin polymerization, leading to the liberation of MRTFs from G-actin and subsequent the nuclear import of MRTFs. SRF-MRTF complex subsequently induces the activation of SRF-dependent transcription of MYH9, and consequently the NMII-A complex. MYH9 could induce the stabilization of tip cell filopodia in order their migration and invasion for new blood formation.

Previously, Franco and colleagues reported a strong regulation of MYL9 (also known as MLC2) expression by SRF and MRTFs. MYL9 depleted cells showed significant defects in endothelial cell migratory behavior (Franco *et al.*, 2013). MYL9 is a regulatory light chain (RLC) of myosin complex (NMII) with several regulatory sites, which enhances the ATPase activity of the non-muscle heavy chain (NMHC), and also promotes an assembly-competent form of non-muscle myosin II (NMII) (Aguilar-Cuenca *et al.*, 2014; Vicente-Manzanares *et al.*, 2009). The activity of NMII is mainly regulated by phosphorylation events of RLCs or NMHCs. Regulation of NMII by RLC phosphorylation depends, fundamentally, on the reversible phosphorylation of the RLC on two highly conserved residues (serine 19 and threonine 18 in vertebrates NMII), increasing the Mg^{2+}-ATPase activity of myosin in the presence of actin. Numerous kinases were described to phosphorylate these residues in diverse regulatory pathways, responding a specific stimulation (including integrin activation by extracellular matrix and cellular ligands, growth factors, cytokines and chemokines). These kinases includes myosin light chain kinase (MLCK; activated by Ca2+/calmodulin), coiled coil-containing kinase (ROCK) citron kinase (both activated by RhoA) and myotonia dystrophyrelated Cdc42-binding kinase (MRCK; activated by Cdc42), among others (Aguilar-Cuenca *et al.*, 2014; Lecuit *et al.*, 2011). Another mode of regulation of NMII involves direct phosphorylation of the NMHC, which destabilizes existing mini-filaments and/or prevents their *de novo* assembly. These events are mediated by proteins of the PKC family as well as stretch-activated calcium channels (TRPMs) that decrease filament formation and alter the subcellular localization of NMII-A (Vicente-Manzanares *et al.*, 2009).

Also, PKC phosphorylation of RLC in Serine 1 and 2 inhibit NMII function, likely by preventing its normal assembly (Aguilar-Cuenca *et al.*, 2014). In our results we observed that the protein levels of pMLC and MLC2 are decreased in SRF and MYH9 deficient HUVECs, suggesting that the Myosin complex is playing a key role in endothelial cells during angiogenesis. However, the molecular mechanisms underlying the control of MYH9 function downstream of VEGF signaling needs to be addressed in the future.

Recently studies, associated NMII-A with cancer cell migration, invasion, and metastasis. High levels of MYH9 is an indicator of a poorer survival, and increased risk of metastasis (Katono *et al.*, 2015; Betapudi *et al.*, 2006). Our study also suggests that MYH9 is an important regulator of sprouting angiogenesis. Therefore, therapeutic strategies targeting MYH9 function could provide a dual beneficial role, preventing both tumor angiogenesis and tumor metastasis.

Future Perspectives

Our study provides a link between SRF-MYH9 in endothelial tip cell function and a novel feature for MYH9 in tip cells filopodia that could be important for sprouting angiogenesis. However, further investigation aiming to define the role of MYH9 (NM-MIIA) during sprouting angiogenesis is needed. We will continue studying the link between SRF and MYH9 in SRF EC-specific KO mouse compared with SRF^{WT} mouse. Additionally, we will use *in vivo* genetic approaches to explore the signaling networks regulating MYH9 function and confirm the importance of MYH9 *in vivo* physiological and pathological angiogenic assays. Thus, in the future our work will focus on:

(1) Study MYH9 EC-specific KO mouse;

(2) Live-imaging of fluorescently-labeled MYH9 spatial and temporal localization in endothelial cells during sprouting angiogenesis using zebrafish embryos;

(3) Investigate the role of myosin contraction in tip cell invasion and also the role of MYH9 in endothelial filopodia formation/stability;

(4) Understand the mechanistic control of MYH9 function by VEGF signaling

V. REFERENCES

Adams, R.H., Alitalo, K. 2007. Molecular regulation of angiogenesis and lymphangiogenesis. Nat. Rev. Mol. Cell Biol. 8: 464–478.

Aguilar-Cuenca, R., Juanes-García, A., Vicente-Manzanares, M. 2014. Myosin II in mechanotransduction: master and commander of cell migration, morphogenesis, and cancer. Cell. Mol. Life Sci. 71: 479–92.

Augustin, H. 2004. Methods in Endothelial Cell Biology. Springer-Verlag Berlin Heidelberg, New York.

Barry, D.M., Xu, K., Meadows, S.M., Zheng, Y., Norden, P.R., Davis, G.E., Cleaver, O. 2015. Cdc42 is required for cytoskeletal support of endothelial cell adhesion during blood vessel formation. Development 142: 3058–3070.

Betapudi, V., Licate, L.S., Egelhoff, T.T. 2006. Distinct roles of nonmuscle myosin II isoforms in the regulation of MDA-MB-231 breast cancer cell spreading and migration. Cancer Res. 66: 4725–4733.

Blacher, S., Erpicum, C., Lenoir, B., Paupert, J., Moraes, G., Ormenese, S., Bullinger, E., Noel, A. 2014. Cell invasion in the spheroid sprouting assay: A spatial organisation analysis adaptable to cell behaviour. PLoS One 9: 1–10.

Blanchoin, L., Boujemaa-Paterski, R., Sykes, C., Plastino, J. 2014. Actin dynamics, architecture, and mechanics in cell motility. Physiol. Rev. 94: 235–63.

Blanco, R., Gerhardt, H. 2013. VEGF and Notch in tip and stalk cell selection. Cold Spring Harb. Perspect. Med. 3: 1–19.

Buchwalter, G., Gross, C., Wasylyk, B. 2004. Ets ternary complex transcription factors. Gene 324: 1–14.

Carmeliet, P. 2003. Angiogenesis in health and disease. Nat. Med. 9: 653–60.

Carmeliet, P. 2005. Angiogenesis in life, disease and medicine. Nature 438: 932–936.

Carmeliet, P. 2000. Mechanisms of angiogenesis and arteriogenesis. Nat. Med. 6: 389–395.

Carmeliet, P., Jain, R.K. 2011. Molecular mechanisms and clinical applications of angiogenesis. Nature 473: 298–307.

Chai, J., Jones, M.K., Tarnawski, A.S. 2004. Serum response factor is a critical requirement for VEGF signaling in endothelial cells and VEGF-induced angiogenesis. FASEB J. 18: 1264–1266.

Clark, K. A., Graves, B.J. 2014. Dual views of SRF: A genomic exposure. Genes Dev. 28: 926–928.

Cochain, C., Channon, K.M., Silvestre, J.S. 2013. Angiogenesis in the Infarcted Myocardium. Antioxid. Redox Signal. 18: 1100-1113.

Eilken, H.M., Adams, R.H. 2010. Dynamics of endothelial cell behavior in sprouting angiogenesis. Curr. Opin. Cell Biol. 22: 617–625.

Esnault, C., Stewart, A., Gualdrini, F., East, P., Horswell, S., Matthews, N., Treisman, R. 2014. Rho-actin signaling to the MRTF coactivators dominates the immediate transcriptional response to serum in fibroblasts. Genes Dev. 28: 943–958.

Fantin, A., Vieira, J.M., Gestri, G., Denti, L., Schwarz, Q., Prykhozhij, S., Peri, F., Wilson, S.W., Ruhrberg, C. 2010. Tissue macrophages act as cellular chaperones for vascular anastomosis downstream of VEGF-mediated endothelial tip cell induction. Blood 116: 829–840.

Fraccaroli, A., Franco, C. A., Rognoni, E., Neto, F., Rehberg, M., Aszodi, A., Wedlich-Söldner, R., Pohl, U., Gerhardt, H., Montanez, E. 2012. Visualization of Endothelial Actin Cytoskeleton in the Mouse Retina. PLoS One 7: 1–9.

Franco, C. A., Blanc, J., Parlakian, A., Blanco, R., Aspalter, I.M., Kazakova, N., Diguet, N., Mylonas, E., Gao-Li, J., Vaahtokari, A., Penard-Lacronique, V., Fruttiger, M., Rosewell, I., Mericskay, M., Gerhardt, H., Li, Z. 2013. SRF selectively controls tip cell invasive behavior in angiogenesis. Development 140: 2321–33.

Franco, C. A., Li, Z. 2009. SRF in angiogenesis: Branching the vascular system. Cell Adhes. Migr. 3: 264–267.

Franco, C.A., Mericskay, M., Parlakian, A., Gary-Bobo, G., Gao-Li, J., Paulin, D., Gustafsson, E., Li, Z. 2008. Serum Response Factor Is Required for Sprouting Angiogenesis and Vascular Integrity. Dev. Cell 15: 448–461.

Fukushima, Y., Okada, M., Kataoka, H., Hirashima, M., Yoshida, Y., Mann, F., Gomi, F., Nishida, K., Nishikawa, S.I., Uemura, A. 2011. Sema3E-PlexinD1 signaling selectively suppresses disoriented angiogenesis in ischemic retinopathy in mice. J. Clin. Invest. 121: 1974–1985.

Gerhardt, H., Golding, M., Fruttiger, M., Ruhrberg, C., Lundkvist, A., Abramsson, A., Jeltsch, M., Mitchell, C., Alitalo, K., Shima, D., Betsholtz, C. 2003. VEGF guides angiogenic sprouting utilizing endothelial tip cell filopodia. J. Cell Biol. 161: 1163–1177.

Geudens, I., Gerhardt, H. 2011. Coordinating cell behaviour during blood vessel formation. Development 138: 4569–4583.

Graupera, M., Potente, M. 2013. Regulation of angiogenesis by PI3K signaling networks. Exp. Cell Res. 319: 1348–1355.

Heckman, C. A., Plummer, H.K. 2013. Filopodia as sensors. Cell. Signal. 25: 2298–2311.

Heinke, J., Patterson, C., Moser, M. 2012. Life is a pattern: vascular assembly within the embryo. Front. Biosci. (Elite Ed). 4: 2269–88.

Hellström, M., Phng, L-K., Hofmann, J.J., Wallgard, E., Coultas, L., Lindblom, P., Alva, J., Nilsson, A-K., Karlsson, L., Gaiano, N., Yoon, K., Rossant, J., Iruela-Arispe, M.L., Kalén, M., Gerhardt, H., Betsholtz, C. 2007. Dll4 signalling through Notch1 regulates formation of tip cells during angiogenesis. Nature 445: 776–80.

Herbert, S.P., Stainier, D.Y.R. 2011. Molecular control of endothelial cell behaviour during blood vessel morphogenesis. Nat. Rev. Mol. Cell Biol. 12: 551–564.

Huang, H., Bhat, A., Woodnutt, G., Lappe, R. 2010. Targeting the ANGPT-TIE2 pathway in malignancy. Nat. Rev. Cancer 10: 575–585.

Iruela-Arispe, M.L., Davis, G.E. 2009. Cellular and Molecular Mechanisms of Vascular Lumen Formation. Dev. Cell 16: 222–231.

Jacquemet, G., Hamidi, H., Ivaska, J. 2015. Filopodia in cell adhesion, 3D migration and cancer cell invasion. Curr. Opin. Cell Biol. 36: 23–31.

Jain, R.K. 2003. Molecular regulation of vessel maturation. Nat. Med. 9: 685–693.

Jakobsson, L., Franco, C. A., Bentley, K., Collins, R.T., Ponsioen, B., Aspalter, I.M., Rosewell, I., Busse, M., Thurston, G., Medvinsky, A., Schulte-Merker, S., Gerhardt, H. 2010. Endothelial cells dynamically compete for the tip cell position during angiogenic sprouting. Nat. Cell Biol. 12: 943–953.

Juanes-Garcia, A., Chapman, J.R., Aguilar-Cuenca, R., Delgado-Arevalo, C., Hodges, J., Whitmore, L. A., Shabanowitz, J., Hunt, D.F., Horwitz, A. R., Vicente-Manzanares, M. 2015. A regulatory motif in nonmuscle myosin II-B regulates its role in migratory front-back polarity. J. Cell Biol. 209: 23–32.

Katono, K., Sato, Y., Jiang, S-X., Kobayashi, M., Nagashio, R., Ryuge, S., Fukuda, E., Goshima, N., Satoh, Y., Saegusa, M., Masuda, N. 2015. Prognostic significance of MYH9 expression in resected non-small cell lung cancer. PLoS One 10: e0121460.

Lamalice, L., Le Boeuf, F., Huot, J. 2007. Endothelial cell migration during angiogenesis. Circ. Res. 100: 782–794.

Lamalice, L., Houle, F., Jourdan, G., Huot, J. 2004. Phosphorylation of tyrosine 1214 on VEGFR2 is required for VEGF-induced activation of Cdc42 upstream of SAPK2/p38. Oncogene 23: 434–45.

Lecuit, T., Lenne, P-F., Munro, E. 2011. Force Generation, Transmission, and Integration during Cell and Tissue Morphogenesis. Annu. Rev. Cell Dev. Biol. 27: 157–184.

Lundquist, M.R., Storaska, A.J., Liu, T.C., Larsen, S.D., Evans, T., Neubig, R.R., Jaffrey, S.R. 2014. Redox modification of nuclear actin by MICAL-2 regulates SRF signaling. Cell 156: 563–576.

Makanya, A.N., Hlushchuk, R., Djonov, V.G.. 2009. Intussusceptive angiogenesis and its role in vascular morphogenesis, patterning, and remodeling. Angiogenesis 12: 113–123.

Manalo, D.J., Rowan, A., Lavoie, T., Natarajan, L., Kelly, B.D., Ye, S.Q., Garcia, J.G.N., Semenza, G.L., Hif-, H. 2005. Transcriptional regulation of vascular endothelial cell responses to hypoxia by HIF-1. Regulation 105: 659–669.

Mattila, P.K., Lappalainen, P. 2008. Filopodia: molecular architecture and cellular functions. Nat. Rev. Mol. Cell Biol. 9: 446–454.

Miano, J.M., Long, X., Fujiwara, K. 2007. Serum response factor: master regulator of the actin cytoskeleton and contractile apparatus. 70-81.

Michaelis, U.R. 2014. Mechanisms of endothelial cell migration. Cell. Mol. Life Sci.: 4131–4148.

Miralles, F., Posern, G., Zaromytidou, A.I., Treisman, R. 2003. Actin dynamics control SRF activity by regulation of its coactivator MAL. Cell 113: 329–342.

Nürnberg, A., Kitzing, T., Grosse, R. 2011. Nucleating actin for invasion. Nat. Rev. Cancer 11: 177–187.

Olson, E.N., Nordheim, A. 2010. Linking actin dynamics and gene transcription to drive cellular motile functions. Nat. Rev. Mol. Cell Biol. 11: 353–365.

Olsson, A-K., Dimberg, A, Kreuger, J, Claesson-Welsh, L. 2006. VEGF receptor signalling - in control of vascular function. Nat. Rev. Mol. Cell Biol. 7: 359–371.

Parsons, JT, Horwitz, A.R., Schwartz, M.A. 2010. Cell adhesion: integrating cytoskeletal dynamics and cellular tension. Nat. Rev. Mol. Cell Biol. 11: 633–643.

Pasapera, A.M., Plotnikov, S.V., Fischer, R.S., Case, L.B., Egelhoff, T.T., Waterman, C.M. 2015. Rac1-Dependent Phosphorylation and Focal Adhesion Recruitment of Myosin IIA Regulates Migration and Mechanosensing. Curr. Biol. 25: 175–186.

Phng, L.K., Gerhardt, H. 2009. Angiogenesis: A Team Effort Coordinated by Notch. Dev. Cell 16: 196–208.

Pitulescu, M.E., Schmidt, I., Benedito, R., Adams, R.H. 2010. Inducible gene targeting in the neonatal vasculature and analysis of retinal angiogenesis in mice. Nat. Protoc. 5: 1518–1534.

Pollard, T.D., Cooper, J.A. 2009. Actin, a central player in cell shape and movement. Science 326: 1208–12.

Posern, G., Sotiropoulos, A., Treisman, R. 2002. Mutant actins demonstrate a role for unpolymerized actin in control of transcription by serum response factor. Mol. Biol. Cell 13: 4167–4178.

Posern, G., Treisman, R. 2006. Actin' together: serum response factor, its cofactors and the link to signal transduction. Trends Cell Biol. 16: 588–596.

Potente, M., Gerhardt, H., Carmeliet, P. 2011. Basic and therapeutic aspects of angiogenesis. Cell 146: 873–887.

Pugh, C.W., Ratcliffe, P.J. 2003. Regulation of angiogenesis by hypoxia: role of the HIF system. Nat. Med. 9: 677–684.

Riedl, J., Flynn, K.C., Raducanu, A., Gärtner, F., Beck, G., Bösl, M., Bradke, F., Massberg, S., Aszodi, A., Sixt, M., Wedlich-Söldner, R. 2010. Lifeact mice for studying F-actin dynamics. Nat. Methods 7: 168–9.

Ruhrberg, C., Gerhardt, H., Golding, M., Watson, R., Ioannidou, S., Fujisawa, H., Betsholtz, C., Shima, D.T. 2002. Spatially restricted patterning cues provided by heparin-binding VEGF-A control blood vessel branching morphogenesis. Genes Dev. 16: 2684–98.

Semenza, G.L. 2003. Angiogenesis in ischemic and neoplastic disorders. Annu. Rev. Med. 54: 17–28.

Siekmann, A.F., Affolter, M., Belting, H.G. 2013. The tip cell concept 10 years after: New players tune in for a common theme. Exp. Cell Res. 319: 1255–1263.

De Smet, F, Segura, I, De Bock, K, Hohensinner, PJ, Carmeliet, P. 2009. Mechanisms of vessel branching: Filopodia on endothelial tip cells lead the way. Arterioscler. Thromb. Vasc. Biol. 29: 639–649.

Strilić, B., Kucera, T., Eglinger, J., Hughes, M.R, McNagny, K.M., Tsukita, S., Dejana, E., Ferrara, N., Lammert, E. 2009. The molecular basis of vascular lumen formation in the developing mouse aorta. Dev. Cell 17: 505–15.

Sun, Q., Chen, G., Streb, J.W., Long, X., Yang, Y., Stoeckert, C.J., Miano, J.M. 2006. Defining the mammalian CArGome. Genome Res. 16: 197–207.

Vestweber, D. 2008. VE-cadherin: The major endothelial adhesion molecule controlling cellular junctions and blood vessel formation. Arterioscler. Thromb. Vasc. Biol. 28: 223–232.

Vicente-Manzanares, M., Ma, X., Adelstein, R.S., Horwitz, A.R. 2009. Non-muscle myosin II takes centre stage in cell adhesion and migration. Nat. Rev. Mol. Cell Biol. 10: 778–790.

Vicente-Manzanares, M., Zareno, J., Whitmore, L., Choi, C.K., Horwitz, A.F. 2007. Regulation of protrusion, adhesion dynamics, and polarity by myosins IIA and IIB in migrating cells. J. Cell Biol. 176: 573–580.

Wang, Z., Wang, D-Z., Pipes, G.C.T., Olson, E.N. 2003. Myocardin is a master regulator of smooth muscle gene expression. Proc. Natl. Acad. Sci. U. S. A. 100: 7129–7134.

Weinl, C., Riehle, H., Park, D., Stritt, C., Beck, S., Huber, G., Wolburg, H., Olson, E.N., Seeliger, M.W., Adams, R.H., Nordheim, A. 2013. Endothelial SRF/MRTF ablation causes vascular disease phenotypes in murine retinae. J. Clin. Invest. 123: 2193–2206.

Yang, C., Svitkina, T. 2011. Filopodia initiation: focus on the Arp2/3 complex and formins. Cell Adh. Migr. 5: 402–408.

Zimna, A., Kurpisz, M. 2015. Hypoxia-Inducible Factor-1 in Physiological and Pathophysiological Angiogenesis: Applications and Therapies. Biomed Res. Int. 2015: 1–13.